Science of the Total Environment 880 (2023) 163260

Contents lists available at ScienceDirect

Science of the Total Environment

journal homepage: www.elsevier.com/locate/scitotenv

Bark beetle impacts on forest evapotranspiration and its partitioning

John F. Knowles [a,*], Nels R. Bjarke [b], Andrew M. Badger [c,1], Max Berkelhammer [d], Joel A. Biederman [e], Peter D. Blanken [f], Mario Bretfeld [g], Sean P. Burns [f,h], Brent E. Ewers [i], John M. Frank [j], Jeffrey A. Hicke [k], Leanne Lestak [l], Ben Livneh [b,c], David E. Reed [m], Russell L. Scott [e], Noah P. Molotch [l]

[a] Department of Earth and Environmental Sciences, California State University, Chico, CA, USA
[b] Department of Civil, Environmental and Architectural Engineering, University of Colorado Boulder, Boulder, CO, USA
[c] Cooperative Institute for Research in Environmental Sciences, University of Colorado Boulder, Boulder, CO, USA
[d] Department of Earth and Environmental Sciences, University of Illinois Chicago, Chicago, IL, USA
[e] Southwest Watershed Research Center, USDA Agricultural Research Service, Tucson, AZ, USA
[f] Department of Geography, University of Colorado Boulder, Boulder, CO, USA
[g] Department of Ecology, Evolution, and Organismal Biology, Kennesaw State University, Kennesaw, GA, USA
[h] National Center for Atmospheric Research, Boulder, CO, USA
[i] Department of Botany and Program in Ecology, University of Wyoming, Laramie, WY, USA
[j] Rocky Mountain Research Station, USDA Forest Service, Fort Collins, CO, USA
[k] Department of Earth and Spatial Sciences, University of Idaho, Moscow, ID, USA
[l] Institute of Arctic and Alpine Research, University of Colorado Boulder, Boulder, CO, USA
[m] Environmental Science, University of Science and Arts of Oklahoma, Chickasha, OK, USA

HIGHLIGHTS

- Post-disturbance *ET* and transpiration (*T*) were quantified by 3 independent methods.
- Bark beetle outbreak reduced *ET* by 2–25 % in the southern Rocky Mountains, USA.
- Initial growing season *T* was 1–31 % relatively more reduced than water year *ET*.
- The VIC model simulated a 9–18 % increase in the post-disturbance runoff ratio.
- *ET* recovery began after 6–8 years but did not fully recover within 10–15 years.

GRAPHICAL ABSTRACT

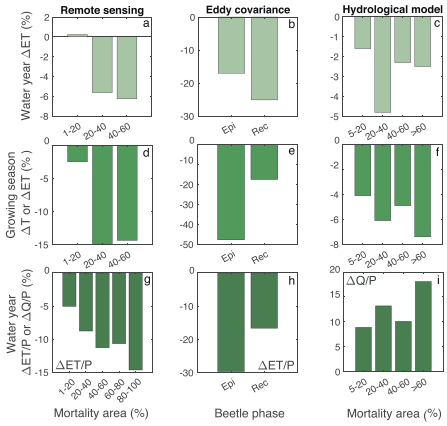

ARTICLE INFO

Editor: Manuel Esteban Lucas-Borja

Keywords:
Water resources
Ecohydrology
Spruce beetle

ABSTRACT

Insect outbreaks affect forest structure and function and represent a major category of forest disturbance globally. However, the resulting impacts on evapotranspiration (*ET*), and especially hydrological partitioning between the abiotic (evaporation) and biotic (transpiration) components of total *ET*, are not well constrained. As a result, we combined remote sensing, eddy covariance, and hydrological modeling approaches to determine the effects of bark beetle outbreak on *ET* and its partitioning at multiple scales throughout the Southern Rocky Mountain Ecoregion (SRME), USA. At the eddy covariance measurement scale, 85 % of the forest was affected by beetles, and water year *ET* as a

* Corresponding author at: Department of Earth and Environmental Sciences, 400 W. First St., Chico, CA 92929-0205, USA.
E-mail address: jfknowles@csuchico.edu (J.F. Knowles).
[1] Now at Cooperative Institute for Satellite Earth System Studies/Earth System Science Interdisciplinary Center, University of Maryland, College Park, MD, USA and Climate Prediction Center, NCEP/NWS/NOAA, College Park, MD, USA.

http://dx.doi.org/10.1016/j.scitotenv.2023.163260
Received 1 December 2022; Received in revised form 10 March 2023; Accepted 31 March 2023
Available online 6 April 2023

GLEES
Niwot Ridge
MODIS

fraction of precipitation (*P*) decreased by 30 % relative to a control site, with 31 % greater reductions in growing season transpiration relative to total *ET*. At the ecoregion scale, satellite remote sensing masked to areas of >80 % tree mortality showed corresponding *ET/P* reductions of 9–15 % that occurred 6–8 years post-disturbance, and indicated that the majority of the total reduction occurred during the growing season; the Variable Infiltration Capacity hydrological model showed an associated 9–18 % increase in the ecoregion runoff ratio. Long-term (16–18 year) *ET* and vegetation mortality datasets extend the length of previously published analyses and allowed for clear characterization of the forest recovery period. During that time, transpiration recovery outpaced total *ET* recovery, which was lagged in part due to persistently reduced winter sublimation, and there was associated evidence of increasing late summer vegetation moisture stress. Overall, comparison of three independent methods and two partitioning approaches demonstrated a net negative impact of bark beetles on *ET*, and a relatively greater negative impact on transpiration, following bark beetle outbreak in the SRME.

1. Introduction

Evapotranspiration (*ET*) regulates both surface water and groundwater recharge and is critically important to water resources (Maxwell and Condon, 2016; Ukkola et al., 2015). Quantifying *ET* represents a key research priority in mountain systems that function as the "water towers of the world" and may be especially vulnerable to climate change (Immerzeel et al., 2020; Viviroli et al., 2011). However, *ET* measurements and models are complicated by spatio-temporally variable controls on both the abiotic surface evaporation and sublimation (*E*) and biotic transpiration (*T*) components of the total *ET* flux (e.g., Roberts, 1983; Kool et al., 2014; Scott et al., 2021; Wei et al., 2017). Moreover, ecological disturbance and resulting land cover changes can alter hydrological partitioning between *E* and *T*, and further between *ET* and streamflow, especially in complex mountain terrain (Chang et al., 2018; Goeking and Tarboton, 2020, 2022; Sterling et al., 2012). A more comprehensive understanding of how vegetation changes affect *ET* and its partitioning is therefore required to accurately simulate mountain ecosystem function and watershed yield following disturbance (e.g., Fisher et al., 2017).

Tree mortality due to bark beetles represents a widespread forest disturbance throughout the southern Rocky Mountains, USA with variable and potentially interactive hydrological consequences (e.g., Burton et al., 2020; Hicke et al., 2016, 2020; Edburg et al., 2012). Bark beetles affect *ET* directly by feeding and reproducing in the phloem of host trees, disrupting nutrient transport and introducing xylem-blocking fungal pathogens (e.g., *Ceratocystis dryocoetidis* Kendrick & Molnar); subsequent host tree mortality results from nutrient and/or water starvation (e.g., McDowell et al., 2011; Raffa et al., 2015). Prior analyses of hydrological sensitivity to bark-beetle-related forest mortality have focused on changes in streamflow that may be indirectly manifested through the hydrological cycle (e.g., Buma and Livneh, 2017; Manning et al., 2022; Ren et al., 2021) or the effects of bark beetle-induced vegetation mortality on *ET* itself (Maness et al., 2012; Vanderhoof and Williams, 2015; Bright et al., 2013; Reed et al., 2014). The current study builds on these results by normalizing *ET* to *P* as a means to disentangle the disturbance effect from interannual meteorological variability that is key to water availability on the landscape and thus hydrological dynamics including *ET* partitioning (Hamlet et al., 2007; Berghuijs et al., 2017).

Bark beetle disturbance results in a sequence of long-term ecohydrological changes. Within one to three years after beetle attack, needles turn red and transpiration ceases (red phase; Hubbard et al., 2013; Frank et al., 2014). After three to five years, most killed trees have lost all remaining needles (gray phase; e.g., Wulder et al., 2006). Following bark beetle outbreak, early research at the watershed scale indicated relatively more hydrological routing to streamflow, in accord with the water balance and expectations of reduced transpiration (Bethlahmy, 1974; Potts, 1984). However, subsequent work showed that increased abiotic evaporation was capable of partially or completely offsetting decreased transpiration (e.g., Biederman et al., 2014, 2015), and that variable outbreak timing can result in co-occurring patches of stand mortality and recovery (Norton et al., 2015; Rhoades et al., 2013), resulting in no net *ET* change or even increased *ET*. The principal competing ecohydrological mechanisms that are responsible for post-disturbance changes in *ET* include changes in leaf area, canopy interception of precipitation, sub-canopy shading, snow accumulation and ablation, albedo, wind speed, and turbulence intensity (Edburg et al., 2012; Mikkelson et al., 2013; Pugh and Gordon, 2012; Reed et al., 2014; Burns et al., 2021). The degree to which each of these processes controls seasonal *ET* and its partitioning throughout the course of forest disturbance and recovery phases remains an open ecohydrological question and represents the focus of the current work (e.g., Rodman et al., 2022).

To address this knowledge gap, the current study utilized a multi-scale research design that incorporated three independent *ET* datasets and two methods to partition *ET* into its constituent parts of transpiration and evaporation. The specific objectives of this study were to (1) quantify the seasonal impacts of bark beetles on *ET* and its partitioning into abiotic *E* versus biotic *T*, (2) determine how these impacts aggregate to modify total annual *ET* during and following outbreak, and (3) evaluate this perturbation within the context of the catchment water balance. To investigate these objectives, we used a multi-scale combination of satellite remote sensing, in situ eddy covariance measurements, and hydrological modeling. By identifying the impact of land cover change due to forest disturbance on regional *ET* and streamflow, this work has broad implications for the hydrological sciences and water resources management communities.

2. Materials and methods

2.1. Remote sensing

2.1.1. Land cover

Satellite remote sensing data were analyzed from areas located between 1500 m and 3947 m above sea level within the 144,462 km^2 Southern Rocky Mountain Ecoregion (SRME; United States Environmental Protection Agency, 2010; Fig. 1a). Analyses were masked to include only areas with evergreen forests as determined by the Landsat-based U.S. Geological Survey (USGS) 2001 National Land Cover Database (NLCD) data (Homer et al., 2004). The NLCD data were upscaled from 30 m to 500 m cell size for consistency with the remotely-sensed *ET* data from the Moderate Resolution Imaging Spectroradiometer (MODIS). Aggregation to 500 m resolution was performed based on the percentage of 30 m NLCD evergreen forest cells inside each 500 m grid cell such that the resulting evergreen mask contained a minimum of 80 % evergreen forest cover. Burned areas that were disturbed between 1985 and 2018 as derived from the MTBS (Monitoring Trends in Burn Severity; www.mtbs.gov) dataset were removed from the evergreen mask. Principal tree species (from approximately north to south) included Engelmann spruce (*Picea engelmanii* Parry ex Engelm.), subalpine fir (*Abies lasioscarpa* (Hook.) Nutt.), lodgepole pine (*Pinus contorta* Douglas ex Loudon), limber pine (*Pinus flexilis* E. James), Douglas-fir (*Pseudotsuga menziesii* (Mirb.) Franco), blue spruce (*Picea pungens* Engelm.), white fir (*Abies concolor* (Gordon & Glend.) Lindl. ex Hildebr.), ponderosa pine (*Pinus ponderosa* ex P. Lawson & C. Lawson), and southwestern white pine (*Pinus strobiformis* Engelm.).

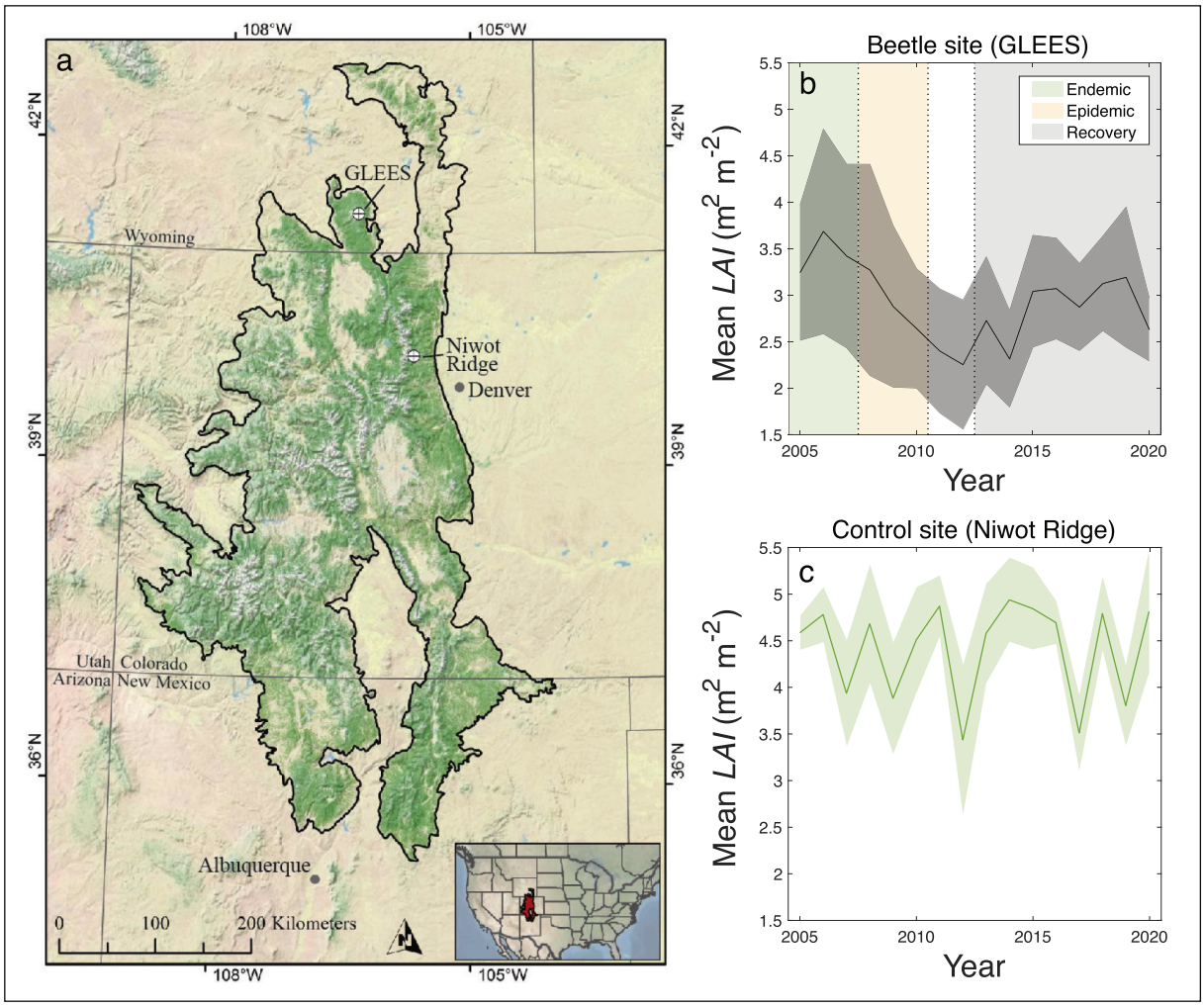

Fig. 1. Site figure shows (a) the EPA Level III Southern Rocky Mountain Ecoregion (outlined in black), forested areas (green), and location of the Niwot Ridge (US-NR1) and GLEES (US-GLE) eddy covariance towers. For context, mean MODIS leaf area index (*LAI*) at (b) the GLEES beetle site during the endemic (water year 2005–2007), epidemic (water year 2008–2010), and recovery (water year 2013–2020) beetle phases (see Section 2.2.4 for beetle phase description) and (c) at the Niwot Ridge control site. Shaded area shows standard deviation among pixels during a four-week period centered on 21 July.

2.1.2. Leaf area index (LAI)

Site-specific *LAI* values were calculated as the mean of four representatively forested MODIS (MCD15A3H) pixels to the west, south, and southeast of the tower at the Glacier Lakes Ecosystem Experiments Site (GLEES; Fig. 1b) or to the north, west, and south of the tower at Niwot Ridge (Fig. 1c), as well as the pixel containing the tower scaffold itself, during the four-week period centered on 21 July that has been previously identified as the period of peak *LAI* at GLEES (Frank et al., 2014). To account for coniferous physiology where stomata cover both sides of the needle leaf, the one-sided MODIS *LAI* projection was multiplied by two to determine the total foliage area per unit ground area (Frank et al., 2014; Chen and Black, 1992).

2.1.3. Mortality area

Mortality area (*MA*) and the year of vegetation mortality were determined from an updated (1997–2018), improved 1 km-resolution cumulative annual dataset derived from United States Forest Service (USFS) Aerial Detection Survey (ADS) data (Hicke et al., 2020). The ADS vegetation mortality data were based on aircraft observations where visual estimates of dead trees were recorded. The year of vegetation mortality was estimated by subtracting one year from the survey date. This 1-year subtraction was necessary given that trees are in the red phase when they are detected and therefore represent the year after beetle attack and subsequent tree death (Holsten et al., 1999; Gibson et al., 2009; Buotte et al., 2016).

2.1.4. Evapotranspiration (ET)

Monthly MODIS-based estimates of *ET* at 500 m resolution were generated by temporal summation of the MODIS 8-day gap-filled *ET* data products (MOD16A2GF v006; Running et al., 2019; Mu et al., 2011). The MODIS *ET* estimates were based on the Penman-Monteith equation forced by both ancillary meteorological data and 8-day MODIS-based vegetation information. The MODIS *ET* product is constructed from four MODIS-based data sources including 8-day composites of Fractional Absorbed Photosynthetically Active Radiation (*FPAR*), 8-day land surface albedo, 8-day Leaf Area Index (*LAI*), and land cover type. The 8-day albedo composites were combined with daily surface solar irradiance and air temperature data from meteorological reanalysis to derive the surface net radiation and ground heat flux (Mu et al., 2011). Surface stomatal conductance and aerodynamic resistance were estimated from a combination of MODIS *LAI* and reanalysis of daily air temperature, vapor pressure deficit, and relative humidity. Biome-dependent vegetation parameters were obtained from MODIS-based land cover information. These parameters were optimized such that annual *ET* estimates agreed with *ET* estimates based on MODIS-derived Gross Primary Productivity (*GPP*) and known water use efficiencies established from eddy covariance measurements (Mu et al., 2011).

MODIS *ET* comparisons to vegetation mortality and precipitation (Parameter-elevation Regressions on Independent Slopes Model; PRISM Climate Group, 2021) were based on mean-aggregated 1 km and 4 km

datasets, respectively, during the period between water years (1 October to 30 September) 2000 and 2017 when both MODIS and *MA* data were applicable. Methodological comparison data were generated by summing monthly changes in *ET* or *T* relative to undisturbed grid cells for the year following disturbance, or as the minimum annual precipitation-normalized *ET* (*ET*/*P*) relative to the pre-disturbance period. Non-parametric Mann-Kendall regression analysis was used to identify temporal forest recovery trends.

2.2. Eddy covariance

The eddy covariance method provides spatially-integrated measurements of surface-atmosphere flux within a representative ecosystem scale statistical measurement footprint (Baldocchi et al., 2001; Chu et al., 2021). This study used eddy covariance to quantify evapotranspiration dynamics at two locations within the SRME, one of which (GLEES) was significantly affected by bark beetles during the study period. Direct eddy covariance measurements of latent heat flux (*LE*) and the net ecosystem exchange of carbon dioxide (*NEE*) were filtered for periods of reduced turbulent mixing and gap-filled by the REddyProc algorithm using a moving "look up" table approach under similar meteorological conditions (Wutzler et al., 2018). Site-specific friction velocity filters were determined by REddyProc as the mean annual friction velocity threshold during the study period (friction velocity threshold = 0.40 m s^{-1} at Niwot Ridge and 0.71 m s^{-1} at GLEES). The *ET* flux was converted from *LE* using the latent heat of vaporization (2.5 × 10^6 J kg^{-1}) and the density of water (1000 kg m^{-3}). Potential *ET* (*PET*) at each site was calculated using the Penman method (Shuttleworth, 1993). Methodological comparison data correspond to the mean between-tower difference between bark beetle outbreak phases at GLEES. Significant differences between eddy covariance sites were evaluated using one-way analysis of variance.

2.2.1. Glacier Lakes Ecosystem Experiments Site (GLEES)

GLEES is located west of Laramie, Wyoming, USA at an elevation of 3190 m above sea level in the Snowy Range Mountains (41°21.992′ N; 106°14.397′ W) (Frank et al., 2014; Speckman et al., 2014). Continuous, ongoing eddy covariance data collection began in 1999 (AmeriFlux ID = US-GLE; doi:10.17190/AMF/1246056), and the long-term mean annual air temperature and precipitation are −2 °C and 1200 mm, respectively. The subalpine forest at this location is comprised of Engelmann spruce and subalpine fir with a median canopy height of 7 m, an interquartile range of 8 m, and a maximum of >30 m; however, trees near the US-GLE scaffold do not generally exceed 18 m. Between 2007 and approximately 2010, the forest experienced an outbreak of spruce beetle (*Dendroctonus rufipennis*), likely due to a lack of minimum wintertime air temperatures below the spruce beetle freeze tolerance threshold (Frank et al., 2014). As a result, healthy tree basal area decreased from 65 m^2 ha^{-1} in 2003 to <10 m^2 ha^{-1} in 2012 (Speckman et al., 2014). Additional eddy covariance data collection and processing details can be found in Frank et al., 2014.

2.2.2. Niwot Ridge

The Niwot Ridge tower (AmeriFlux ID = US-NR1; doi:10.17190/AMF/1246088) is located in the subalpine forest approximately 25 km west of Boulder, Colorado, USA and 8 km east of the Continental Divide at 3050 m above sea level (40°1′58.4″ N; 105°32′47.0″ W). Continuous, ongoing eddy covariance data collection began at this location in November 1998, and the long-term mean annual air temperature and precipitation are 1.3 °C and 698 mm, respectively (Knowles et al., 2015), which is warmer and drier than GLEES. The mixed coniferous forest consists of lodgepole pine, subalpine fir, and Engelmann spruce, and the mean canopy height was 11.5 m in 2002 (Turnipseed et al., 2002). Although bark beetles are endemic to this location, <6 % of the trees around the tower had been affected by beetles by 2013 (Moore et al., 2013); therefore, we used this site as a control with which to establish the effect of beetles on *ET* and the transpiration fraction of *ET* via paired tower analysis with GLEES. Additional specifics about the instrumentation, data collection, and processing at Niwot Ridge can be found in Burns et al. (2016).

2.2.3. Transpiration partitioning

The transpiration fraction of *ET* (*T*/*ET*) was determined using an "optimal approach" that assumes close correlation between rates of ecosystem transpiration and *GPP*, i.e., the stomatal-driven components of an ecosystem's water and carbon fluxes derived from eddy covariance data (Berkelhammer et al., 2016; Zhou et al., 2016). For this analysis, *GPP* was modeled using the measured *NEE* and a soil temperature response function to extrapolate nighttime respiration values throughout the daytime hours (Reichstein et al., 2005). Both *ET* and *GPP* were subsequently normalized by vapor pressure deficit (*VPD*), which linearizes the relationship between *ET* and *GPP* and is analogous to water use efficiency (Zhou et al., 2014), and a second-order power law function was used to describe the relationship between the 5th percentile of *ET* and normalized, binned *GPP*. The 5th percentile of *ET* was used in favor of the minimum *ET* because the singular *ET* minimum within a bin is often an outlier resultant from noise or bias in the gas analyzer or uncertainty in the model used to derive *GPP* from *NEE* (Berkelhammer et al., 2016; Zhou et al., 2016). In this way, *ET* in excess of the minimum value within each bin must be associated with the abiotic component of the latent heat flux i.e., evaporation from bare soil or leaf surfaces. The *T*/*ET* analysis was restricted to midday conditions (incoming solar radiation >600 W m^{-2}), and the 30-min *T*/*ET* data were generated separately for every water year to account for potential changes in the transpiration-*GPP* relationship with progressive vegetation mortality.

2.2.4. Beetle outbreak phases and hydrological seasons

Eddy covariance data from both sites were parsed into endemic (water years 2005–2007), epidemic (water years 2008–2010), and recovery (water years 2013–2020) phases corresponding to before, during, and after the occurrence of epidemic bark beetle populations and associated widespread tree mortality at GLEES (Frank et al., 2014). Water years 2011 and 2012 were the wettest and driest on record at each site, respectively, and because these years also spanned the epidemic-to-recovery phase transition, they were excluded from the eddy covariance analysis to avoid confounding interpretation of results. Recognizing that seasons defined by month inconsistently capture critical changes in moisture availability, time-varying snow accumulation, snowmelt, and summer drydown "hydrological seasons" were characterized at each site. For this analysis, the snow accumulation and snowmelt seasons were separated by the first of five consecutive days when soil moisture increased above its winter (DJF) average for that water year (Koehn et al., 2021). Similarly, the break between the snowmelt and summer drydown seasons (when soil moisture is determined by rainfall) was characterized as the first day after the peak snowmelt pulse when soil moisture was less than the summer (JJA) mean for that water year (Koehn et al., 2021). To obtain a continuous soil moisture record, the GLEES soil moisture variable was calculated as the average of up to seven sensors, each located at 10 cm depth. The Niwot Ridge soil moisture variable was calculated as the average of soil moisture at 5 cm and 10 cm depth (1 sensor at each depth).

2.3. Hydrological model

The Variable Infiltration Capacity (VIC; Liang et al., 1994) Version 5 land surface model is a physically based model that is able to reconcile spatio-temporally dynamic processes in complex terrain (Nijssen et al., 1997, 2001). The VIC model additionally includes mosaic land cover to capture sub-grid variability in vegetation classes, an important element in this study with which to aid representation of sub-grid variability in vegetation mortality. Within VIC, *ET* was dynamically computed from Penman-Monteith *PET* (Monteith, 1973), modified by stomatal and architectural vegetation resistance terms, and coupled to annual MODIS-derived vegetation parameters (Bohn and Vivoni, 2019) to evaluate changes in water and energy balances. Updated daily precipitation, maximum and minimum air temperature, and wind forcings were used in conjunction with an offline

MTCLIM algorithm to force the hydrologic simulation at a daily time step (Hungerford et al., 1989; Livneh et al., 2015a). Non-vegetation land-surface parameterizations for the model were derived from the Mizukami et al. (2017) regionalized parameter set and were subsequently re-gridded from 1/8° to 1/16° spatial resolution. To ensure that subsurface water and climatology had sufficient time to equilibrate, a spin-up simulation incorporated meteorological forcings from 1950 to 1999 and served as the initial condition for successive water year simulations to represent vegetation change due to bark beetles.

Annual VIC simulations were performed between water years 2000 and 2016 for all grid cells with >80 % forest cover throughout the SRME, in accord with the remote sensing component of this study. Low disturbance grid cells (*MA* < 5 %; 852 grid cells) served as a baseline distribution for relative comparison to increasingly disturbed grid cells, in order to reduce uncertainty associated with spatial heterogeneity throughout the study domain. We specifically analyzed four disturbance classes corresponding to *MA* = 5–20 % (707 grid cells), 20–40 % (329 grid cells), 40–60 % (85 grid cells), and >60 % (27 grid cells) where *MA* and the year of vegetation mortality were determined from Hicke et al. (2020) as in the remote sensing analysis. Post-disturbance hydrological anomalies were calculated on a grid cell by grid cell basis as the mean value during the time-varying post-disturbance period relative to the mean value during the time-varying pre-disturbance period. Methodological comparison data represent the median of the modeled distribution for the various combinations of hydrological fluxes and disturbance classes. All distributions were tested for statistically significant differences from the baseline using a non-parametric Mann-Whitney two-sample test.

3. Results and discussion

3.1. Remote sensing

3.1.1. Beetle outbreak and recovery timeline

During the 15–16 years following bark beetle outbreak (length of record varies by disturbance bin), *ET/P* initially decreased but then showed signs of recovery (Fig. 2). In addition, the flashiness of the post-disturbance *ET/P* response generally increased with mortality area (*MA*) such that *ET/P* from more disturbed areas (higher *MA*) both decreased and recovered more rapidly than *ET/P* from less disturbed areas (lower *MA*). During the months of June, July, and August (JJA), growing season *ET* normalized by water year (*WY*) *P* (*ET/P*) decreased by a maximum of 1 % (*MA* = 1–20 %), 4 % (*MA* = 20–40 %), 5 % (*MA* = 40–60 % and 60–80 %), or 7 % (*MA* = 80–100 %) relative to the pre-disturbance period (Fig. 2a). The minimum growing season *ET/P* occurred 5–8 years after the onset of disturbance, and there was a significant ($0.003 > p > 0.06$) positive *ET/P* recovery trend for all *MA* disturbance classes thereafter (Fig. 2a). Growing season *ET/P* from more disturbed areas recovered faster than *ET/P* from less disturbed areas such that growing season *ET/P* from the most severely disturbed (*MA* = 80–100 %) areas had completely recovered within 14 years.

Water year *ET/P* closely paralleled trends in growing season *ET/P* following disturbance, and decreased by a maximum of 5 % (*MA* = 1–20 %), 9 % (*MA* = 20–40 %), 11 % (*MA* = 40–60 % and 60–80 %), or 15 % (*MA* = 80–100 %) relative to the pre-disturbance period (Fig. 2b). Dividing by the minimum *WY* Δ*ET/P*, changes in JJA *ET/P* thus accounted for 20 % (*MA* = 1–20 %), 44 % (*MA* = 20–40 %), 45 % (*MA* = 40–60 % and 60–80 %), or 47 % (*MA* = 80–100 %) of *WY ET/P* reductions. For moderate-to-severely disturbed areas (*MA* > 20 %), minimum annual *ET/P* occurred 6–8 years after the onset of disturbance, and there was a significant positive *ET/P* recovery trend for the majority of *MA* disturbance classes thereafter: 20–40 % ($p = 0.01$), 40–60 % ($p = 0.03$), 60–80 % ($p = 0.12$), and 80–100 % ($p = 0.04$) (Fig. 2b). The minimum *ET/P* in less disturbed areas (*MA* < 20 %) occurred 15 years after the onset of disturbance and indicates that disturbance may not have been sufficient to represent the dominant control on WY *ET* during that time (Adams et al., 2011). At the end of the study period, *WY ET/P* ranged from <1 % to 9 % below pre-disturbance levels, and there was evidence of an inverse relationship between disturbance severity and magnitude of recovery consistent with growing season dynamics (Fig. 2b).

Previous MODIS-based work characterized maximum growing season *ET* reductions of 13–44 % (Colorado, USA; Bright et al., 2013) and 19 % (British Columbia, Canada; Maness et al., 2012) following bark beetle outbreak. The current study shows that MODIS-based growing season *ET/P* was reduced by <1–7 % following bark beetle outbreak, and that recovery continued for 10 years after the minimum value at a pace that was mediated by the severity of disturbance (Anderegg et al., 2016; Fig. 2a). This trajectory of post-beetle *ET* decline and recovery aligns with previous work in the SRME where the minimum MODIS *ET* occurred 6 years post-disturbance (Bright et al., 2013). A subsequent study that coupled MODIS *ET* with dendrochronology to extend this line of research through time suggested that growing season *ET* took 21–30 years to recover to pre-disturbance levels in the SRME (Vanderhoof and Williams, 2015). Here,

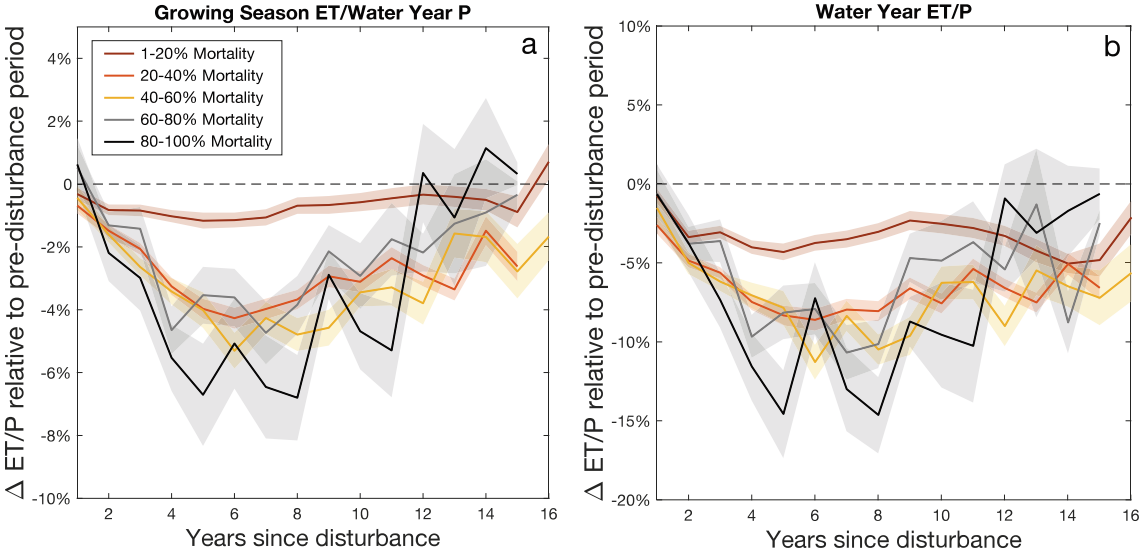

Fig. 2. Remote sensing analysis shows how the ratio of *ET* to precipitation (*P*) changes as a function of time and disturbance severity following beetle outbreak during (a) the growing season (JJA) and (b) the water year in the Southern Rocky Mountain Ecoregion. Shaded areas denote the standard error among *ET* values in each disturbance class. Note the different y-axis scales between panels.

we demonstrate that forest *ET/P* recovery varies as a function of disturbance severity with more disturbed areas recovering at a faster pace than less disturbed areas.

Given that JJA Δ*ET/P* accounted for 44–47 % of maximum *WY ET/P* reductions (*MA* > 20 %), and recognizing that the growing season extends into spring and fall (i.e., beyond JJA; Knowles et al., 2020), it is likely that growing season *ET/P* changes were the major contributor to total post-disturbance Δ*ET/P* (Fig. 2). This result corresponds to the magnitude of transpiration that represents a majority of *ET* in needle-leaf ecosystems (Wei et al., 2017), and supports an overriding biotic effect on *ET* following bark beetle outbreak relative to potentially competing abiotic processes (e.g., Goeking and Tarboton, 2020; Frank et al., 2019). Similarities between observed *ET/P* recovery trajectories during the peak growing season and water year corroborate the importance of growing season processes, and constrain the effect of vegetation regrowth on the annual water balance (Collins et al., 2011). However, we acknowledge increased uncertainty with disturbance severity in Fig. 2, especially above *MA* = 60 %, and suspect that the actual Δ*ET/P* differences between disturbance classes may be more gradual. Contributing factors to unexpected differences between the *MA* curves in Fig. 2 include smaller bin sizes for the more severe disturbance classes (42 total pixels for *MA* > 60 %) and/or potentially misclassified pixels in the *MA* dataset (Hicke et al., 2020). Problematic satellite retrievals during the winter (e.g., Tian et al., 2004), species invariant representation of stomatal conductance (e.g., Ewers et al., 2005), and/or changing vegetation parameters with mortality (e.g., Frank et al., 2014) are also potential sources of uncertainty in the MODIS *ET* algorithm and thus the WY *ET/P* results.

3.1.2. Disturbance effects on monthly ET

To further constrain feedbacks between disturbance severity and the timing and magnitude of hydrological response, monthly changes in MODIS *ET* during the year following identification of disturbance were binned by disturbance class and analyzed with respect to undisturbed areas (*MA* = 0–5 %; Fig. 3). Peak monthly *ET* changes occurred in June (*MA* = 5–20 %; Δ*ET* = −2 mm) or July (*MA* = 20–40 % and *MA* = 40–60 %; Δ*ET* = −8 mm), and *ET* was persistently reduced relative to undisturbed areas between April and September. During this period, *ET* reductions from moderately (*MA* = 20–40 %) and severely (*MA* = 40–60 %) disturbed areas were similar with a total Δ*ET* of −28 mm for both disturbance classes. JJA *ET* reductions from moderately and severely disturbed areas were also similar (Δ*ET* = −20 mm) and thus represented 71 % of the April–September growing season effect. Accordingly, monthly *ET* analysis reinforces the dominant contribution of growing season processes to the annual water budget (Fig. 2), and corroborates an *MA* threshold of 20 % for significant hydrological change to occur (Adams et al., 2011; Stednick, 1996). For *MA* > 20 %, relative insensitivity of growing season *ET* to *MA* may be emerging as characteristic of seasonally water-limited systems like the SRME (e.g., Andrus et al., 2018; Fahey and Knight, 1986) where transpiration is much lower than its potential rate such that excess water available due to tree death is readily consumed by remaining vegetation (Ren et al., 2021; Norton et al., 2015; Bretfeld et al., 2021). During the remainder of the year, post-disturbance *ET* was modified by minor gains (Feb–Apr; *MA* = 5–20 %) and losses (Oct–Nov; *MA* = 40–60 %) corresponding to shoulder season biotic effects and/or initial abiotic changes prior to the onset of widespread canopy defoliation (e.g., Edburg et al., 2012).

3.2. Eddy covariance

3.2.1. Annual trends

To account for potentially confounding topographical and meteorological spatial variability throughout the SRME, 16 years of eddy covariance *ET* data from regionally co-located bark beetle (GLEES, WY) and control (Niwot Ridge, CO) sites were analyzed over the course of a bark beetle outbreak at GLEES (Fig. 4). During the endemic phase, GLEES mean annual *ET* (769 mm; $p = 0.02$) and *ET/PET* (0.34; $p = 0.05$) were significantly higher than Niwot Ridge (*ET* = 578 mm; *ET/PET* = 0.21), but *ET* and *ET/PET* at GLEES decreased to 665 mm and 0.26 during the beetle epidemic itself, whereas the Niwot Ridge values remained similar (*ET* = 594 mm; *ET/PET* = 0.22). Between-site *ET* differences were no longer significant during the epidemic phase, but *ET/PET* ($p = 0.02$) continued to be significantly higher at GLEES. During the first three years of the recovery phase, *ET* (536 mm) and *ET/PET* (0.21) reached their minimum annual values at GLEES and were lower than but not significantly different from Niwot Ridge. However, both the GLEES *ET* ($p = 0.005$) and *ET/PET* ($p = 0.008$) rebounded and were significantly higher than Niwot Ridge during the following five years of recovery (years 4–8 following the end of the epidemic phase). Overall, the mean annual recovery phase *ET* and *ET/PET* at GLEES and Niwot Ridge were 561 mm and 0.23 compared to 543 mm and 0.21, respectively. Throughout all phases of the bark beetle outbreak, mean annual *ET/P* was significantly higher at Niwot Ridge than GLEES ($0.005 < p < 0.09$), but the mean *ET/P* difference between sites was 30 % greater during the epidemic phase and 17 % greater during the recovery phase relative to pre-disturbance (endemic) conditions.

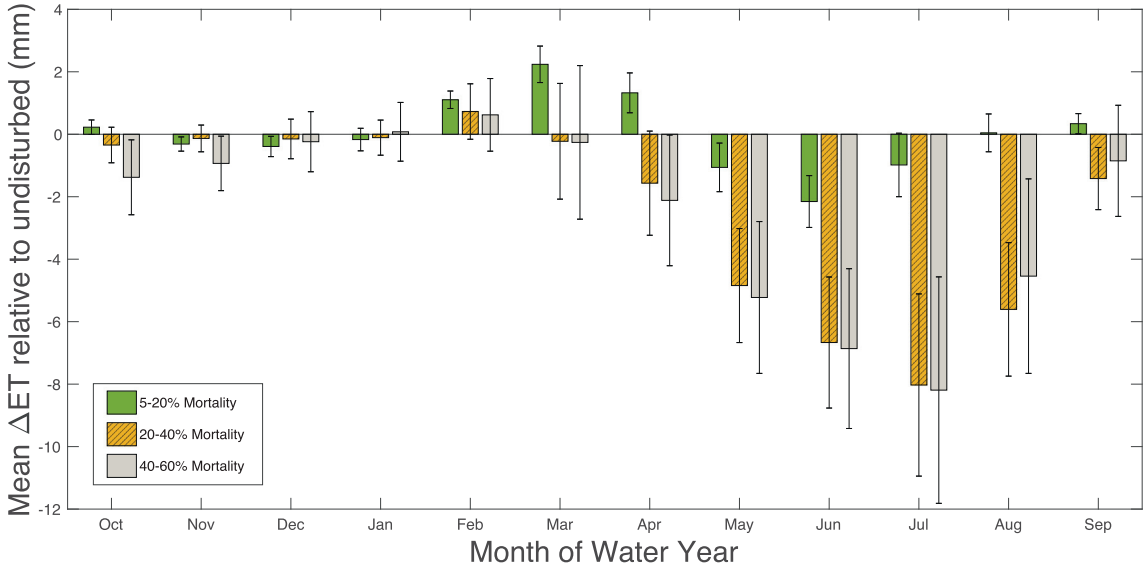

Fig. 3. The mean and variability (standard error) of the monthly MODIS *ET* difference between undisturbed (<5 % mortality) and disturbed (binned by severity of disturbance) areas during the year following identification of beetle disturbance.

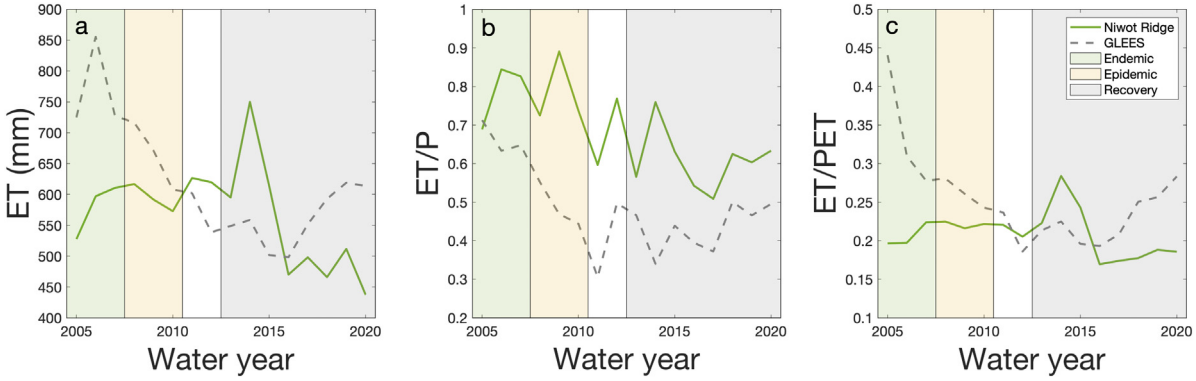

Fig. 4. Eddy covariance (a) evapotranspiration (*ET*), (b) *ET* as a fraction of precipitation (*P*), and (c) *ET* as a fraction of total annual potential *ET* (*PET*) over time at Niwot Ridge and GLEES. All data correspond to water year annual sums.

Continuous eddy covariance monitoring for 16 years before, during, and after a bark beetle outbreak extends the length of previous in situ growing season *ET* analyses in the SRME by a decade or more (Frank et al., 2014). Mean annual *ET* at GLEES was suppressed during the outbreak until approximately 6 years post-disturbance when there was evidence of a recovery trend. This time frame agrees with the remote sensing results and provides an independent constraint on the pace of *ET* recovery. Both tower- and satellite-based results aligned with a strong initial growth response of advance regeneration (trees <2.5 cm DBH and >3 years old at the time of disturbance) to reduced canopy cover that has been shown to occur 6–8 years post-disturbance in a variety of conifer forests, especially in unharvested stands that represent the majority of beetle-killed area in the SRME (Collins et al., 2011; Gandhi et al., 2022; Norton et al., 2015; Bretfeld et al., 2021). Relative differences in *ET* and *ET/PET* versus *ET/P* dynamics between sites demonstrate how changes in canopy characteristics may differentially alter patterns of energy and water use throughout the course of a bark beetle outbreak (Fig. 1b; Brown et al., 2014; Reed et al., 2014); precipitation measurement uncertainty may have also affected the *ET/P* calculation (e.g., Burns et al., 2015). Similarly, higher baseline *ET* at GLEES may reflect differences in site meteorology, species composition (spruce-dominated vs. pine-dominated), or other forest characteristics (Frank et al., 2016; Knowles et al., 2017).

3.2.2. Seasonal trends

Seasonal analysis adds context to the processes responsible for observed trends in mean annual *ET* during each disturbance phase. Pre-disturbance, GLEES *ET* was higher than Niwot Ridge *ET* during every month with a maximum difference between sites in midsummer and midwinter (Fig. 5a). During the beetle epidemic, the mean monthly *ET* disparity between sites was reduced during all months except January and February, and the GLEES *ET* became lower than the Niwot Ridge *ET* in May, June, and July. As disturbance progressed from the endemic to the epidemic phase, the maximum cross-site mean monthly *ET* difference occurred in June ($\Delta ET = -36$ mm) and July ($\Delta ET = -30$ mm), which broadly corresponds to the snowmelt season that is critical to annual productivity in the SRME (Hu et al., 2010; Knowles et al., 2018). A negligible impact of beetles on cross-site *ET* differences during January and February reflects an expected lack of sublimation response during the epidemic phase before trees lose their needles, as opposed to the recovery phase when maximum cross-site differences in *ET* relative to the epidemic phase in January ($\Delta ET = -12$ mm) and February ($\Delta ET = -15$ mm) coincided with needlefall and decreased canopy interception (Frank et al., 2019; Molotch et al., 2007). Relative to the endemic phase, cross-site *ET* reductions were progressively greater during the recovery phase than the epidemic phase during all periods except the peak growing season months of June, July, and August, which

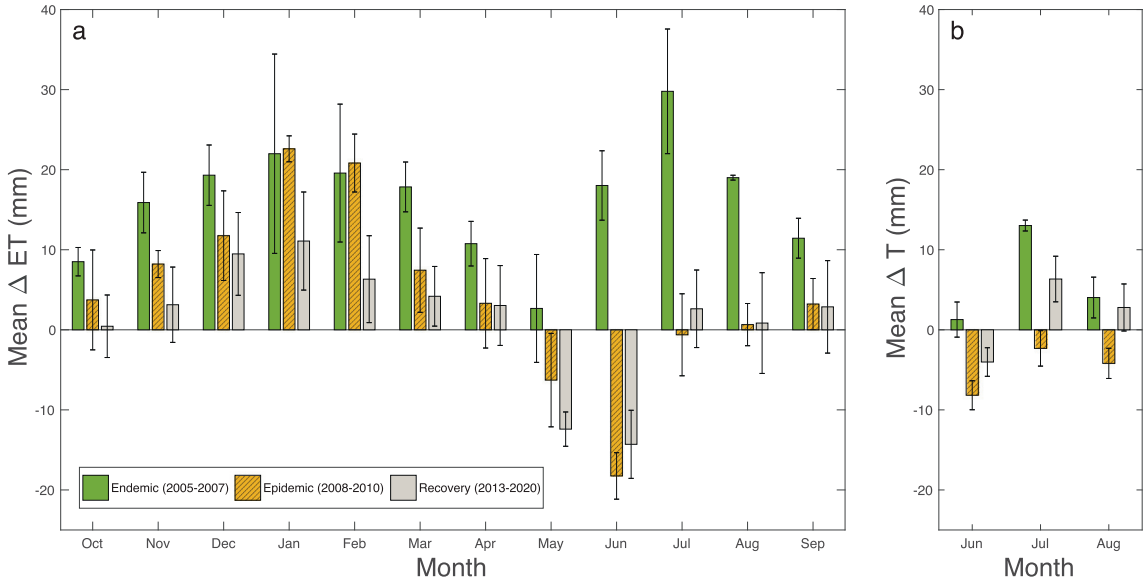

Fig. 5. The monthly total eddy covariance (a) evapotranspiration (*ET*) and (b) transpiration (*T*) difference between GLEES and Niwot Ridge changes with beetle phase throughout the water year. Mean annual differences were calculated as GLEES minus Niwot Ridge such that positive values correspond to a higher magnitude at GLEES and negative values are a higher magnitude at Niwot Ridge. Error bars are the standard error of the annual difference during each phase.

corroborates a growth response of remaining vegetation during this time (Collins et al., 2011). Overall, the minimum and maximum mean monthly differences between the endemic and recovery beetle phases at GLEES and Niwot Ridge occurred in April ($\Delta ET = -8$ mm) and June ($\Delta ET = -32$ mm), respectively.

A transpiration partitioning algorithm was applied to the eddy covariance data in order to isolate the effect of beetles on the abiotic evaporation versus biotic transpiration (*T*) components of the total *ET* flux (Zhou et al., 2016; Section 2.2.3; Fig. 5b). During the peak growing season months of June, July, and August, endemic phase *T* at GLEES was 1 mm, 13 mm, and 4 mm higher than Niwot Ridge and accounted for 7 %, 44 %, and 21 % of the total *ET* difference between sites. Greater between-site differences in *T*/*ET* during the late summer months of July and August supports that the later melting and relatively deeper infiltrating snowpack at GLEES significantly reduces the potential for moisture limitation to late season vegetation productivity that has been observed at Niwot Ridge (Knowles et al., 2018; Winchell et al., 2016). In spite of this, the epidemic phase *T* at GLEES decreased to 8 mm, 2 mm, and 4 mm lower than Niwot Ridge during June, July, and August when reduced *T* accounted for 26 %, 50 %, and 45 % of the total observed *ET* reduction between sites. Recovery phase *T* increases during June, July, and August were 0.2 mm, 5 mm, and 5 mm greater than the corresponding changes in total *ET* relative to the epidemic phase, which implies that biotic *T* recovery compensated for reduced abiotic *E* up to a decade post-disturbance, and was the mechanism behind ecosystem *ET* recovery.

3.2.3. Changes in forest function

Sixteen years of simultaneous, continuous eddy covariance data collection at Niwot Ridge and GLEES allows for process-based evaluation of changing limitation to *ET* as a function of disturbance phase (Fig. 6). For this purpose, we specifically leveraged soil moisture data to separate and compare *ET* and *PET* during the time-varying snow accumulation (vegetation dormant; *ET* energy limited), snowmelt (vegetation active; *ET* energy limited), and soil drydown (vegetation active; *ET* energy or moisture limited) "hydrological seasons" at each site (Koehn et al., 2021; Section 2.2.4). At the Niwot Ridge control site, there was no significant relationship between *ET* and *PET* during the snow accumulation period (Fig. 6a). However, during the snowmelt and drydown seasons when *ET* and *PET* were significantly correlated, it was expected that the relationship between *ET* and *PET*, expressed as the slope of the corresponding linear regression, would not change significantly between beetle disturbance phases. This expectation was substantiated during the snowmelt period (Fig. 6b), but not during the soil drydown period when recovery phase *ET* was significantly ($p = 0.04$; analysis of covariance) less sensitive to changes in *PET* relative to both the endemic and epidemic phases (Fig. 6c). Although Niwot Ridge was not subjected to the beetle epidemic, this result suggests altered forest function in 2013–2020 relative to 2005–2010, potentially due to legacy effects of the 2012 drought on vegetation or moisture carryover that would be expected to manifest during the soil drydown period (Chen et al., 2015; Dannenberg et al., 2022; Knowles et al., 2018).

During the snow accumulation season at GLEES, *ET* and *PET* were negatively correlated during the endemic phase, but not significantly related during the epidemic and recovery phases (Fig. 6d). Mechanistically, observed post-disturbance insensitivity of *ET* to *PET* supports the idea that reductions in canopy-intercepted snow (sublimates very efficiently) following beetle outbreak counteracted reduced shading on the snowpack surface and higher within-canopy wind speeds, which reinforces the importance of canopy sublimation to the total sublimation flux (Frank et al., 2019; Sexstone et al., 2018). During the snowmelt season, the sensitivity of *ET* to *PET* decreased during the epidemic phase ($p = 0.002$), but then rebounded albeit with a lower intercept ($p < 0.001$) during the recovery phase, likely due to the reduction in leaf area associated with the death of mature trees (Fig. 6e). Although the *ET* sensitivity to *PET* did not change with beetle phase during the soil drydown season, the recovery phase intercept was similarly reduced ($p = 0.03$) relative to the endemic phase, in accord with a canopy regeneration signal and leaf area limitation to transpiration (Fig. 6f). Comparing *ET* vs. *PET* between the snowmelt and soil drydown portions of the growing

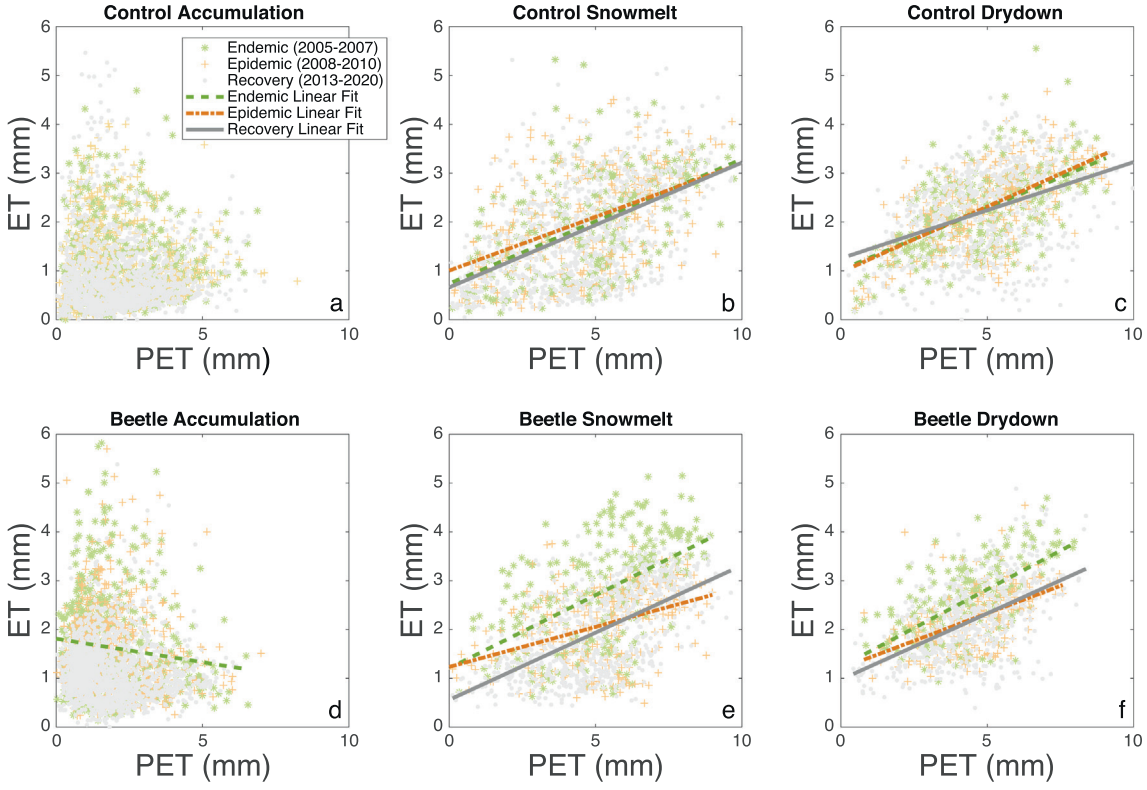

Fig. 6. Daily eddy covariance evapotranspiration (*ET*) as a function of potential evapotranspiration (*PET*) during the snow accumulation, snowmelt, and drydown hydrological seasons at Niwot Ridge (top row, "control") and GLEES (bottom row, "beetle") as defined by intra-annual soil moisture dynamics following Koehn et al., 2021. Lines denote corresponding linear relationships that are significant at $p < 0.05$.

season, *ET* shifted to become less sensitive to *PET* ($p = 0.02$) during the recovery phase drydown season only, indicating that disturbance and associated changes in the age distribution and/or health of remaining vegetation may have exacerbated late summer moisture limitation to *ET* at GLEES (Andrus et al., 2018; Paine et al., 1998; Au et al., 2022).

3.3. VIC hydrological model

Comparison of measured and modeled results affords an independent assessment of process understanding and can be used to develop future lines of research inquiry and/or model improvements (e.g., Wieder et al., 2017). In the current study, modeling analysis additionally allows for simulation of how changes in land cover and *ET* translate to changes in post-disturbance streamflow (*Q*) that are critical to effective water resource management (Barnhart et al., 2021; Livneh et al., 2015b). As such, we modeled changes in *ET*, *T*, and the runoff ratio (*Q*/*P*) throughout the SRME as a means to complement satellite remote sensing and eddy covariance data, as well as to identify potential knowledge gaps in process understanding or representation.

3.3.1. Changes in ET and transpiration

The median modeled water year *ET* from disturbed areas ranged from 2 to 5 % less than *ET* from low disturbance (*MA* < 5 %) grid cells (Fig. 7a). Reduced post-disturbance *ET* broadly aligned with observational trends, but both modeled and remotely sensed *ET* reductions were an order of magnitude less than the eddy covariance results (see Section 3.4 below), and the model unexpectedly produced a maximum *ET* reduction for *MA* = 20–40 % relative to any other disturbance class. This difference underscores the difficulties of working at large spatial scales, especially in complex terrain where gradients in water availability and vegetation type and mortality occur over short horizontal and vertical distances and may be inconsistently correlated with disturbance (e.g., Thayer et al., 2018; Tai et al., 2019). At these scales, errors due to incomplete representation of the ecohydrological system are exacerbated by the potential for divergent ecosystem response to model forcing data; the resultant multivariate heterogeneity is manifested in the long distribution tails of the VIC modeling results that are indicative of a potential signal-to-noise problem where disturbance-induced hydrological changes (i.e., "the signal") can be difficult to distinguish from inter-annual background hydrological variability (i.e., "the noise") (Fig. 7; Knowles et al., 2017; Livneh et al., 2015a). In addition, modeled *ET* reductions may be conservative as a result of the spin-up period that preceded the Millennium drought in the southwestern USA (Cayan et al., 2010). Accordingly, modeling studies based on tower forcing data are more closely aligned with the eddy covariance results of the current study e.g., Chen et al. (2015) determined 22 % less *ET* following the bark beetle outbreak at GLEES.

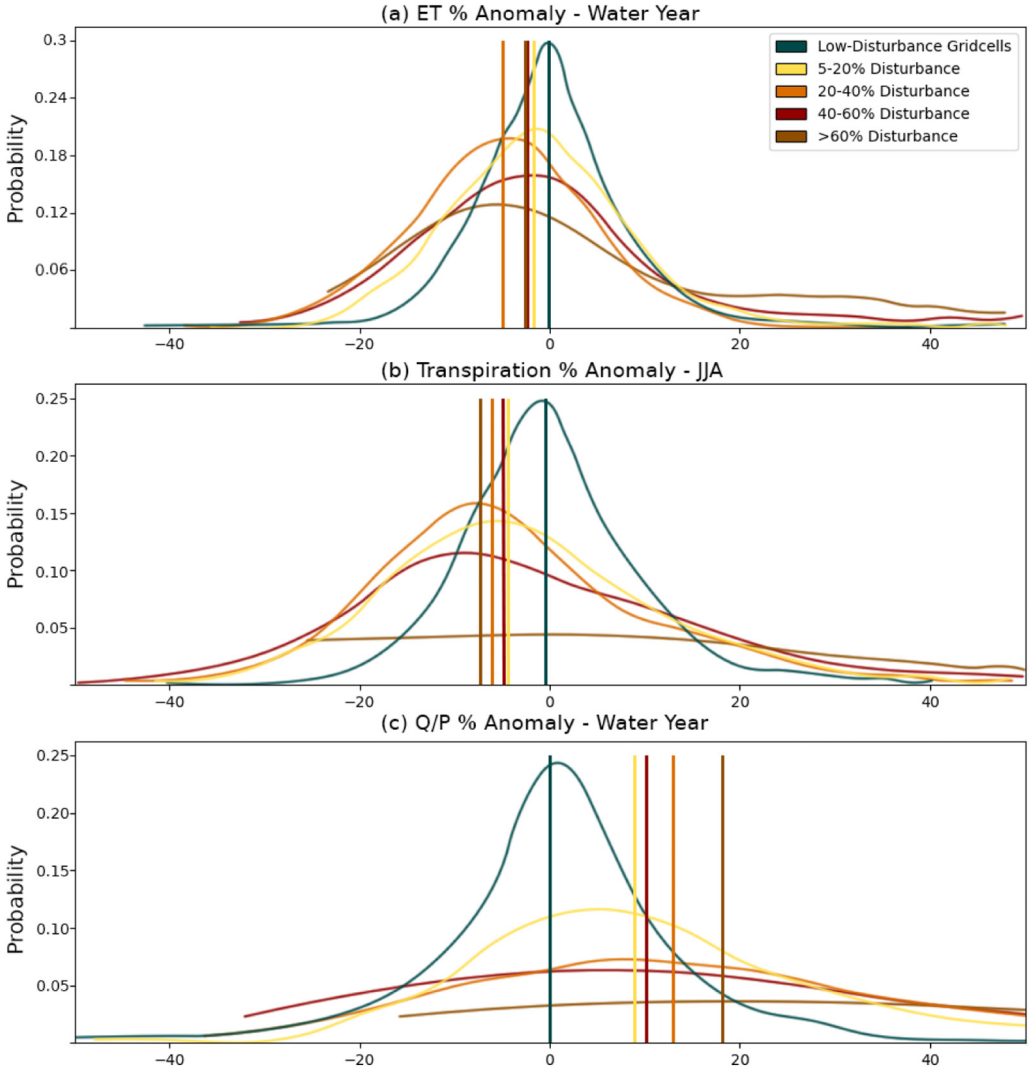

Fig. 7. VIC-modeled Kernel Density Estimates (KDEs) of (a) water year *ET*, (b) growing season (JJA) transpiration, and (c) water year runoff ratio (*Q*/*P*) anomalies corresponding to beetle disturbance classes of increasing severity. Median values of each distribution are shown as vertical lines and were significantly different ($p < 0.01$; non-parametric two-sample Mann-Whitney test) from the low disturbance distribution.

Modeled transpiration changes were greater than water year *ET* changes and indicated that negative biotic effects overwhelmed any potentially compensating abiotic effects on *ET* (Fig. 7b). Specifically, median modeled *T* values during the months of June, July, and August were 4 %, 6 %, 5 %, and 7 % less than low disturbance (*MA* < 5 %) grid cells for disturbance classes of *MA* = 5–20 %, 20–40 %, 40–60 %, and >60 %, respectively (Fig. 7b). The corresponding *T/ET* decreased by 0.4 (*MA* > 25 %) and 0.3 (*MA* > 40 %) standard deviations from the mean, respectively. Relatively stable *T* anomalies above *MA* = 20 % were consistent with the remote sensing component of our analysis and could be indicative of an aridity effect that supersedes the sensitivity of *ET* to vegetation mortality area (Ren et al., 2021). In addition, relative insensitivity of modeled *T* to increasing mortality could represent an artifact of the time-varying model experimental design where it is possible for the post-disturbance period to span periods of compensatory *T* and *ET* dynamics (i.e., the epidemic and recovery phases) for grid cells that were disturbed near the beginning of the study (Liang et al., 2016). In this way, ecosystem recovery may have inhibited the model's ability to isolate nearer-term from longer-term disturbance effects on both *T* and *ET* (e.g., Rhoades et al., 2013). Overall, modeled *T* reductions throughout the SRME were modest relative to bark beetle *ET* studies at smaller ecosystem or regional spatial scales (e.g., 13–44 % less growing season *ET* following disturbance; Bright et al., 2013; Chen et al., 2015), which reinforces the effect of spatio-temporal heterogeneity associated with ecosystem characteristics and/or disturbance on the ecoregion-scale model results.

3.3.2. Changes in the runoff ratio

We utilized the VIC model to quantitatively translate bark beetle impacts into changes in runoff (Fig. 7c). Accordingly, median modeled water year runoff ratios were 9 %, 13 %, 10 %, and 18 % more than low disturbance (*MA* < 5 %) grid cells for disturbance classes of *MA* = 5–20 %, 20–40 %, 40–60 %, and >60 %, respectively (Fig. 7c). Modeled runoff ratio anomalies exceeded both *ET* and *T* anomalies and were consistent with a previous catchment-scale modeling study in the SRME (*Q/P* increased by 8–13 %; Livneh et al., 2015b). However, the VIC modeling distributions spanned a wide range of solutions including fluxes of the opposite sign for all modeled hydrological outputs, and thereby emphasize heterogeneity within the SRME study domain that integrates disturbance effects across myriad combinations of soil, vegetation, climatology, and elevation representative of semi-arid regions (Fig. 7). As such, previous studies that determined no change or a decreased runoff ratio following bark beetle outbreak may be indicative of particular locations, sets of circumstances, and/or time periods within the SRME (e.g., Biederman et al., 2014, 2015; Guardiola-Claramonte et al., 2011; Slinski et al., 2016). Overall, the current results broadly support an emerging paradigm of ecohydrological variability along multiple axes with respect to prediction and interpretation of post-disturbance hydrological response (Goeking and Tarboton, 2020). In particular, the SRME is generally characterized by higher aridity than more northerly regions that have contributed significantly to current understanding (e.g., Cudmore et al., 2010; Maness et al., 2012) with subsequent differences in snow accumulation and melt characteristics, vegetation physiology and structure, and spatial heterogeneity that are among the strongest known predictors of post-disturbance water yield (Goeking and Tarboton, 2022; Manning et al., 2022; Ren et al., 2021).

3.4. Methodological comparison

Recognizing that each method has a unique set of advantages, disadvantages, and biases, we compared remote sensing, eddy covariance, and hydrological model approaches to quantify post-disturbance changes in *ET*, *T*, *ET/P*, and *Q/P* following bark beetle outbreak (Fig. 8). Above *MA* =

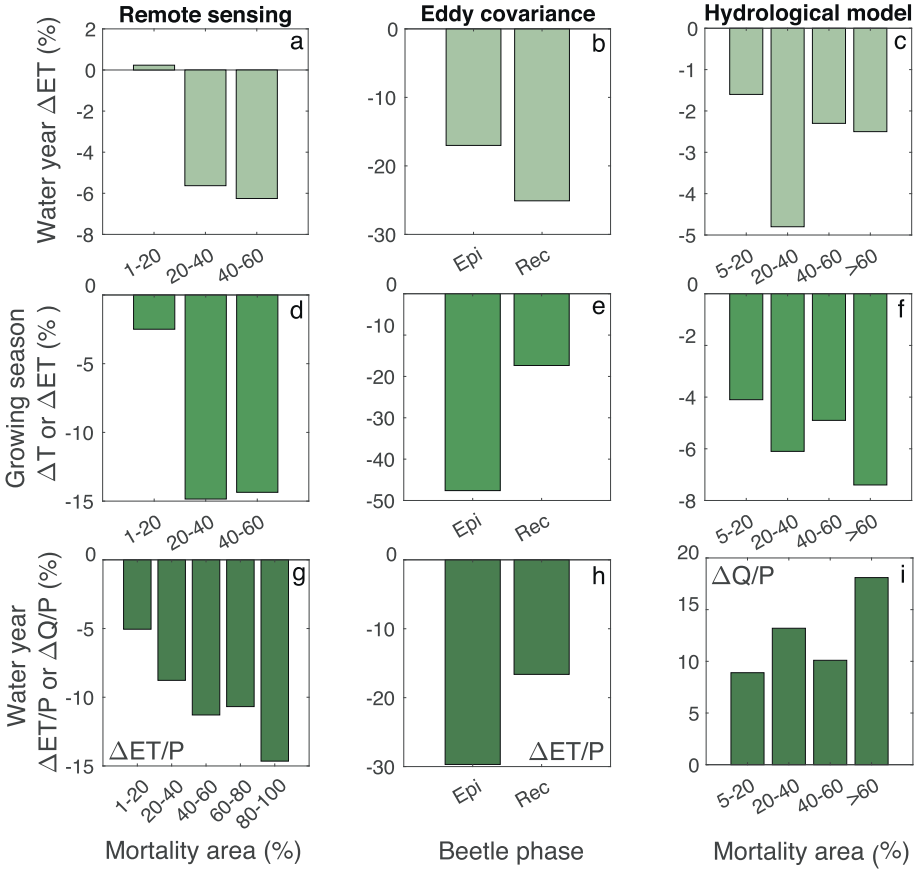

Fig. 8. Summary of ecohydrological changes due to bark beetle outbreak indicated by (left column) remote sensing, (middle column) eddy covariance, and (right column) hydrological modeling analyses. Changes are expressed relative to undisturbed or low disturbance conditions (details in Sections 2.1–2.3) as a function of mortality area or beetle phase where "Epi" is epidemic and "Rec" is recovery.

20 % (i.e., excluding the marginal remote sensing ΔET increase for MA = 1–20 %), all three methods demonstrated a net negative effect on post-disturbance *ET*, ranging from 2 to 25 % (Fig. 8a–c). Further, all methods indicated that changes in *ET* were primarily due to changes in *T* (or growing season *ET*), which decreased 5–48 % relative to pre-disturbance conditions above the MA = 20 % threshold (Fig. 8d–f). For both *T* and *ET*, the hydrological model analysis was the least sensitive to disturbance, the eddy covariance measurements were the most sensitive, and remote sensing was in between. Normalizing *ET* by precipitation increased the magnitude of the remotely sensed disturbance effect by 56 % (MA = 20–40 %) to 81 % (MA = 40–60 %) relative to the non-normalized estimate (*ET*), and thus demonstrates how interannual precipitation variability can both affect ecosystem response and mask surface-driven ecohydrological trends (Fig. 8g; Manning et al., 2022; Ren et al., 2021). However, normalizing the eddy covariance-based *ET* by precipitation changed the timing but not the magnitude of the disturbance effect, i.e., the maximum effect was realized during the epidemic (*ET/P*) as opposed to the recovery (*ET*) beetle phase (Fig. 8h). The VIC hydrological model showed 9–18 % more water allocated to runoff (higher runoff ratios) following disturbance, with the size of the effect generally proportional to vegetation mortality area, in accord with expected propagation of *ET* and *T* reductions through the water balance (Fig. 8i).

Differences between remotely sensed, in situ, and modeled estimates of *ET*, *T*, and *ET/P* can be attributed to differences in both spatial domain and experimental design. For example, the remote sensing and modeling analyses were performed at 1 km or 4 km resolution and do not therefore capture the fine scale topographical and ecohydrological complexity characteristic of the heterogeneous SRME study domain. Consequently, these analyses were less sensitive to disturbance than the eddy covariance method that leveraged a paired tower approach to isolate the disturbance signal from confounding terrain or other factors. Increased measurement fidelity, however, comes with a significant spatial representativeness tradeoff relative to the larger study domain where evergreen forest cover is often less dense and/or continuous (Homer et al., 2004). Remote sensing and modeling approaches are also subject to particular limitations associated with species composition, seasonality, and beetle phase (Ewers et al., 2005; Tian et al., 2004; Frank et al., 2014). Moreover, it was not possible to replicate the same experimental setup among the various methods due to differences in data availability and methodological capabilities that necessitated the use of different time periods, disturbance classes, and statistical techniques. Notwithstanding, accounting for key methodological differences, three independent approaches converged to demonstrate broadly consistent epidemic and recovery dynamics of *ET* and *T* following bark beetle outbreak in the SRME.

4. Conclusion

We applied three independent methods to address a currently open ecohydrological question: How does bark beetle outbreak affect *ET* and its partitioning? All three methods indicated a post-disturbance *ET* reduction with the model also simulating proportionally increased runoff. Both remote sensing and eddy covariance data also converged to estimate a maximum post-disturbance *ET* decrease approximately 6–8 years after beetle attack and a recovery trend thereafter, consistent with an advance regeneration growth response to reduced canopy cover. Process-based analysis of the eddy covariance data uncovered a similar canopy regeneration signal, and the same analysis showed that post-disturbance *ET* became less sensitive to *PET* as snowmelt moisture availability decreased, indicating that bark beetle outbreak intensified moisture limitation to *ET* during the late summer drydown period. During the winter, there was a negligible impact of disturbance on winter *ET* (sublimation) during the epidemic/red phase, but a much stronger negative impact during the recovery/gray phase that was associated with decreased canopy interception following canopy defoliation. Overall, 10–15 years of post-disturbance observational *ET* data was not long enough to capture full ecosystem recovery at the ecosystem or ecoregion scale.

Two transpiration partitioning approaches showed that *T* decreased relatively more than *ET* and therefore suggested that *T* was a primary mechanism by which bark beetle outbreak reduced overall *ET*. Although the current SRME bark beetle outbreak has subsided, bark beetles are endemic to forested areas globally, and there will be more outbreaks in the future. Given widespread increasing aridity, reduced *ET* and the subsequent recovery timeline demonstrated by this work will be subject to modification by increased potential for water limitation that may supersede or ameliorate bark beetle impacts if moisture becomes sufficiently limiting to *ET*. As a result, additional efforts to parse the heterogeneous study domain by elevation or aridity index will be needed to estimate the potential severity of this effect; forthcoming higher resolution (30-m) data products such as OpenET will likely be key to achieving this goal and reducing uncertainty associated with predictions of bark beetle impacts on *ET*. However, the current study leveraged broad agreement between multiple independent measurement and modeling approaches to characterize the magnitude and duration of post-disturbance *ET* changes at multiple scales throughout the SRME. These results have implications for water resources and land management at multiple scales during and following forest disturbance associated with insect-related mortality, and support the emerging paradigm that nuanced interpretation is required to accurately predict post-disturbance hydrological impacts in areas of complex terrain.

CRediT authorship contribution statement

John F. Knowles: Conceptualization, Methodology, Formal analysis, Writing – original draft, Writing – review & editing, Visualization, Supervision, Project administration, Funding acquisition. **Nels R. Bjarke:** Methodology, Formal analysis, Writing – review & editing, Visualization. **Andrew M. Badger:** Methodology, Formal analysis, Writing – review & editing, Visualization. **Max Berkelhammer:** Software, Writing – review & editing. **Joel A. Biederman:** Methodology, Writing – review & editing. **Peter D. Blanken:** Investigation, Writing – review & editing. **Mario Bretfeld:** Investigation, Data curation, Writing – review & editing. **Sean P. Burns:** Investigation, Data curation, Writing – review & editing. **Brent E. Ewers:** Investigation, Writing – review & editing. **John M. Frank:** Investigation, Data curation, Writing – review & editing. **Jeffrey A. Hicke:** Resources, Writing – review & editing. **Leanne Lestak:** Methodology, Software, Formal analysis, Data curation, Writing – review & editing, Visualization. **Ben Livneh:** Methodology, Resources, Supervision, Writing – review & editing. **David E. Reed:** Writing – review & editing. **Russell L. Scott:** Writing – review & editing, Funding acquisition. **Noah P. Molotch:** Conceptualization, Methodology, Resources, Writing – review & editing, Supervision, Funding acquisition.

Data availability

Data used in this manuscript are available from the original data providers as indicated in the text.

Declaration of competing interest

The authors declare that they have no known competing financial interests or personal relationships that could have appeared to influence the work reported in this paper.

Acknowledgements

This research was supported by Colorado Water Institute funding to J.F. Knowles and N.P. Molotch (Colorado Water Conservation Board award #5365761) and to J.F. Knowles from the U.S. Department of Energy Office of Science through the AmeriFlux Management Project.

References

Adams, H.D., Luce, C.H., Breshears, D.D., Allen, C.D., Weiler, M., Hale, V.C., Smith, A.M.S., Huxman, T.E., 2011. Ecohydrological consequences of drought and infestation triggered tree dieoff: insights and hypotheses. Ecohydrology 5 (2), 145–159. https://doi.org/10.1002/eco.233.

Anderegg, W.R.L., Martinez-Vilalta, J., Cailleret, M., Camarero, J.J., Ewers, B.E., Galbraith, D., Gessler, A., Grote, R., Huang, C.-Y., Levick, S.R., Powell, T.L., Rowland, L., Sánchez-Salguero, R., Trotsiuk, T., 2016. When a tree dies in the forest: scaling climate-driven tree mortality to ecosystem water and carbon fluxes. Ecosystems 19, 1133–1147. https://doi.org/10.1007/s10021-016-9982-1.

Andrus, R.A., Harvey, B.J., Rodman, K.C., Hart, S.J., Veblen, T.T., 2018. Moisture availability limits subalpine tree establishment. Ecology 99, 567–575. https://doi.org/10.1002/ecy.2134.

Au, T.F., Maxwell, J.T., Robeson, S.M., Li, J., Siani, S.M.O., Novick, K.A., Dannenberg, M.P., Phillips, R.P., Li, T., Chen, Z., Lenoir, J., 2022. Younger trees in the upper canopy are more sensitive but also more resilient to drought. Nat. Clim. Chang. 12, 1168–1174. https://doi.org/10.1038/s41558-022-01528-w.

Baldocchi, D.D., Falge, E., Gu, L., Olson, R., Hollinger, D., Running, S., Anthoni, P., Bernhofer, C., Davis, K., Evans, R., Fuentes, J.D., Goldstein, A.H., Katul, G.G., Law, B.E., Lee, X., Malhi, Y., Meyers, T., Munger, J.W., Oechel, W.C., Paw U, K.T., Pilegaard, K., Schmid, H.P., Valentini, R., Verma, S.B., Vesala, T., Wilson, K., Wofsy, S.C., 2001. FLUXNET: a new tool to study the temporal and spatial variability of ecosystem-scale carbon dioxide, water vapor, and energy flux densities. Bull. Am. Meteorol. Soc. 82, 2415–2434.

Barnhart, T.B., Vukomanovic, J., Bourgeron, P., Molotch, N.P., 2021. Future land cover and climate may drive decreases in snow wind-scour and transpiration, increasing streamflow at a ColoradoUSA headwater catchment. Hydrol. Process. 35, e14416. https://doi.org/10.1002/hyp.14416.

Berghuijs, W.R., Larsen, J.R., van Emmerik, T.H.M., Woods, R.A., 2017. A global assessment of runoff sensitivity to changes in precipitation, potential evaporation, and other factors. Water Resour. Res. 53, 8475–8486. https://doi.org/10.1002/2017WR021593.

Berkelhammer, M., Noone, D.C., Wong, T.E., Burns, S.P., Knowles, J.F., Kaushik, A., Blanken, P.D., Williams, M.W., 2016. Convergent approaches to determine an ecosystem's transpiration fraction. Glob. Biogeochem. Cycles 30, 933–951. https://doi.org/10.1002/2016GB005392.

Bethlahmy, N., 1974. More streamflow after a bark beetle epidemic. J. Hydrol. 23, 185–189. https://doi.org/10.1016/0022-1694(74)90001-8.

Biederman, J.A., Harpold, A.A., Gochis, D.J., Ewers, B.E., Reed, D.E., Papuga, S.A., Brooks, P.D., 2014. Increased evaporation following widespread tree mortality limits streamflow response. Water Resour. Res. 50, 5395–5409. https://doi.org/10.1002/2013WR014994.

Biederman, J.A., Somor, A.J., Harpold, A.A., Gutmann, E.D., Breshears, D.D., Troch, P.A., Gochis, D.J., Scott, R.L., Meddens, A.J.H., Brooks, P.D., 2015. Recent tree die-off has little effect on streamflow in contrast to expected increases from historical studies. Water Resour. Res. 51, 9775–9789. https://doi.org/10.1002/2015WR017401.

Bohn, T.J., Vivoni, E.R., 2019. MOD-LSP, MODIS-based parameters for hydrologic modeling of North American land cover change. Sci. Data 6, 144. https://doi.org/10.1038/s41597-019-0150-2.

Bretfeld, M., Speckman, H.N., Beverly, D.P., Ewers, B.E., 2021. Bayesian predictions of bark beetle attack and mortality of three conifer species during epidemic and endemic populations stages. Front.For.Glob.Chang. 4. https://doi.org/10.3389/ffgc.2021.679104.

Bright, B.C., Hicke, J.A., Meddens, A.J.H., 2013. Effects of bark beetle-caused tree mortality on biogeochemical and biogeophysical MODIS products. J. Geophys. Res. Biogeosci. 118, 974–982. https://doi.org/10.1002/jgrg.20078.

Brown, M.G., Black, T.A., Nesic, Z., Foord, V.N., Spittlehouse, D.L., Fredeen, A.L., Bowler, R., Grant, N.J., Burton, P.J., Trofymow, J.A., Lessard, D., Meyer, G., 2014. Evapotranspiration and canopy characteristics of two lodgepole pine stands following mountain pine beetle attack. Hydrol. Process. 28, 3326–3340. https://doi.org/10.1002/hyp.9870.

Buma, B., Livneh, B., 2017. Key landscape and biotic indicators of watersheds sensitivity to forest disturbance identified using remote sensing and historical hydrography data. Environ. Res. Lett. 12. https://doi.org/10.1088/1748-9326/aa7091.

Buotte, P.C., Hicke, J.A., Preisler, H.K., Abatzoglou, J.T., Raffa, K.F., Logan, J.A., 2016. Climate influences on whitebark pine mortality from mountain pine beetle in the Greater Yellowstone Ecosystem. Ecol. Appl. 26, 2507–2524. https://doi.org/10.1002/eap.1396.

Burns, S.P., Blanken, P.D., Turnipseed, A.A., Hu, J., Monson, R.K., 2015. The influence of warm-season precipitation on the diel cycle of the surface energy balance and carbon dioxide at a Colorado subalpine forest site. Biogeosciences 12, 7349–7377. https://doi.org/10.5194/bg-12-7349-2015.

Burns, S.P., Frank, J.M., Massman, W.J., Patton, E.G., Blanken, P.D., 2021. The effect of static pressure-wind covariance on vertical carbon dioxide exchange at a windy subalpine forest site. Agric. For. Meteorol. 306, 108402. https://doi.org/10.1016/j.agrformet.2021.108402.

Burns, S.P., Maclean, G.D., Blanken, P.D., Oncley, S.P., Semmer, S.R., Monson, R.K., 2016. The Niwot Ridge Subalpine Forest US-NR1 AmeriFlux site - part 1: data acquisition and site record-keeping. Geosci. Instrum. Method. Data Syst. 5, 451–471. https://doi.org/10.5194/gi-5-451-2016.

Burton, P.J., Jentsch, A., Walker, L.R., 2020. The ecology of disturbance interactions. Bioscience 70, 854–870. https://doi.org/10.1093/biosci/biaa088.

Cayan, D.R., Das, T., Pierce, D.W., Barnett, T.P., Tyree, M., Gershunov, A., 2010. Future dryness in the southwest US and the hydrology of the early 21st century drought. Proc. Natl. Acad. Sci. 107, 21271–21276. https://doi.org/10.1073/pnas.0912391107.

Chang, L.-L., Dwivedi, R., Knowles, J.F., Fang, Y.-H., Niu, G.-Y., Pelletier, J.D., Rasmussen, C., Durcik, M., Barron-Gafford, G.A., Meixner, T., 2018. Why do large-scale land surface models produce a low ratio of transpiration to evapotranspiration? J. Geophys. Res. Atmos. 123, 9109–9130. https://doi.org/10.1029/2018JD029159.

Chen, F., Zhang, G., Barlage, M., Zhang, Y., Hicke, J.A., Meddens, A., Zhou, G., Massman, W.J., Frank, J., 2015. An observational and modeling study of impacts of bark beetle-caused tree mortality on surface energy and hydrological cycles. J. Hydrometeorol. 16, 744–761. https://doi.org/10.1175/JHM-D-14-0059.1.

Chen, J.M., Black, T.A., 1992. Defining leaf area index for non-flat leaves. Plant Cell Environ. 15, 421–429. https://doi.org/10.1111/j.1365-3040.1992.tb00992.x.

Chu, H., Luo, X., Ouyang, Z., Chan, W.S., Dengel, S., Biraud, S.C., Torn, M.S., Metzger, S., Kumar, J., Arain, M.A., Arkebauer, T.J., Baldocchi, D., Bernacchi, C., Billesbach, D., Black, T.A., Blanken, P.D., Bohrer, G., Bracho, R., Brown, S., Brunsell, N.A., Chen, J., Chen, X., Clark, K., Desai, A.R., Duman, T., Durden, D., Fares, S., Forbrich, I., Gamon, J.A., Gough, C.M., Griffis, T., Helbig, M., Hollinger, D., Humphreys, E., Ikawa, H., Iwata, H., Ju, Y., Knowles, J.F., Knox, S.H., Kobayashi, H., Kolb, T., Law, B., Lee, X., Litvak, M., Liu, H., Munger, J.W., Noormets, A., Novick, K., Oberbauer, S.F., Oechel, W., Oikawa, P., Papuga, S.A., Pendall, E., Prajapati, P., Prueger, J., Quinton, W.L., Richardson, A.D., Russell, E.S., Scott, R.L., Starr, G., Staebler, R., Stoy, P.C., Stuart-Haëntjens, E., Sonnentag, O., Sullivan, R.C., Suyker, A., Ueyama, M., Vargas, R., Wood, J.D., Zona, D., 2021. Representativeness of Eddy-covariance flux footprints for areas surrounding AmeriFlux sites. Agric. For. Meteorol. 301–302, 108350. https://doi.org/10.1016/j.agrformet.2021.108350.

Collins, B.J., Rhoades, C.C., Hubbard, R.M., Battaglia, M.A., 2011. Tree regeneration and future stand development after bark beetle infestation and harvesting in Colorado lodgepole pine stands. For. Ecol. Manag. 261, 2168–2175. https://doi.org/10.1016/j.foreco.2011.03.016.

Cudmore, T.J., Björklund, N., Carroll, A., Lindgren, B.S., 2010. Climate change and range expansion of an aggressive bark beetle: evidence of higher beetle reproduction in naïve host tree populations. J. Appl. Ecol. 47, 1036–1043. https://doi.org/10.1111/j.1365-2664.2010.01848.x.

Dannenberg, M.P., Yan, D., Barnes, M.L., Smith, W.K., Johnston, M.R., Scott, R.L., Biederman, J.A., Knowles, J.F., Wang, X., Duman, T., Litvak, M.E., Kimball, J.S., Williams, A.P., Zhang, Y., 2022. Exceptional heat and atmospheric dryness amplified losses of primary production during the 2020 U.S.Southwest hot drought. Glob. Chang. Biol. 28, 4794–4806. https://doi.org/10.1111/gcb.16214.

Edburg, S.L., Hicke, J.A., Brooks, P.D., Pendall, E.G., Ewers, B.E., Norton, U., Gochis, D., Gutmann, E.D., Meddens, A.J., 2012. Cascading impacts of bark beetle-caused tree mortality on coupled biogeophysical and biogeochemical processes. Front. Ecol. Environ. 10, 416–424. https://doi.org/10.1890/10173.

Ewers, B.E., Gower, S.T., Bond-Lamberty, B., Wang, C.K., 2005. Effects of stand age and tree species on canopy transpiration and average stomatal conductance of boreal forests. Plant Cell Environ. 28, 600–678. https://doi.org/10.1111/j.1365-3040.2005.01312.x.

Fahey, T.J., Knight, D.H., 1986. Lodgepole pine ecosystems. Bioscience 36, 610–617. https://doi.org/10.2307/1310196.

Fisher, J.B., Melton, F., Middleton, E., Hain, C., Anderson, M., Allen, R., McCabe, M.F., Hook, S., Baldocchi, D., Townsend, P.A., Kilic, A., Tu, K., Miralles, D.D., Perret, J., Lagouarde, J.-P., Waliser, D., Purdy, A.J., French, A., Schimel, D., Famiglietti, J.S., Stephens, G., Wood, E.F., 2017. The future of evapotranspiration: global requirements for ecosystem functioning, carbon and climate feedbacks, agricultural management, and water resources. Water Resour. Res. 53, 2618–2626. https://doi.org/10.1002/2016WR020175.

Frank, J.M., Massman, W.J., Ewers, B.E., Huckaby, L.S., Negron, J.F., 2014. Ecosystem CO2/H2O fluxes are explained by hydraulically limited gas exchange during tree mortality from spruce bark beetles. J. Geophys. Res. Biogeosci. 119, 1195–1215. https://doi.org/10.1002/2013JG002597.

Frank, J.M., Massman, W.J., Ewers, B.E., Williams, D.G., 2019. Bayesian analyses of 17 winters of water vapor fluxes show bark beetles reduce sublimation. Water Resour. Res. 55, 1598–1623. https://doi.org/10.1029/2018WR023054.

Frank, J.M., Massman, W.J., Swiatek, E., Zimmerman, H.A., Ewers, B.E., 2016. All sonic anemometers need to correct for transducer and structural shadowing in their velocity measurements. J. Atmos. Ocean. Technol. 33, 149–167. https://doi.org/10.1175/JTECH-D-15-0171.1.

Gandhi, K.J.K., Miller, C.N., Fornwalt, P.J., Frank, J.M., 2022. Bark beetle outbreaks alter biotic components of forested ecosystems. Bark Beetle Management, Ecology, and Climate Change. Elsevier, pp. 227–259 https://doi.org/10.1016/B978-0-12-822145-7.00008-8.

Gibson, K., Kegley, S., Bentz, B., 2009. Forest Insect and Disease Leaflet 2: Mountain Pine Beetle. USDA Forest Service, Portland, OR, USA.

Goeking, S.A., Tarboton, D.G., 2022. Variable streamflow response to forest disturbance in the Western US: a large-sample hydrology approach. Water Resour. Res. 58. https://doi.org/10.1029/2021WR031575.

Goeking, S.A., Tarboton, D.G., 2020. Forests and water yield: a synthesis of disturbance effects on streamflow and snowpack in western coniferous forests. J. For. 118, 172–192. https://doi.org/10.1093/jofore/fvz069.

Guardiola-Claramonte, M., Troch, P.A., Breshears, D.D., Huxman, T.E., Switanek, M.B., Durcik, M., Cobb, N.S., 2011. Decreased streamflow in semi-arid basins following drought-induced tree die-off: a counter-intuitive and indirect climate impact on hydrology. J. Hydrol. 406, 225–233. https://doi.org/10.1016/j.jhydrol.2011.06.017.

Hamlet, A.F., Mote, P.W., Clark, M.P., Lettenmaier, D.P., 2007. Twentieth-century trends in runoff, evapotranspiration, and soil moisture in the western United States. J. Clim. 20, 1468–1486. https://doi.org/10.1175/JCLI4051.1.

Hicke, J.A., Meddens, A.J.H., Kolden, C.A., 2016. Recent tree mortality in the Western United States from bark beetles and forest fires. For. Sci. 62, 141–153. https://doi.org/10.5849/forsci.15-086.

Hicke, J.A., Xu, B., Meddens, A.J.H., Egan, J.M., 2020. Characterizing recent bark beetle-caused tree mortality in the western United States from aerial surveys. For. Ecol. Manag. 475, 118402. https://doi.org/10.1016/j.foreco.2020.118402.

Holsten, E.H., Thier, R.W., Munson, A.S., Gibson, K.E., 1999. Forest Insect and Disease Leaflet 127: The Spruce Beetle. USDA Forest Service, Washington, DC, USA.

Homer, C., Huang, C., Yang, L., Wylie, B., Coan, M., 2004. Development of a 2001 National Land-Cover Database for the United States. Photogramm. Eng. Remote Sens. 70, 829–840. https://doi.org/10.14358/PERS.70.7.829.

Hu, J., Moore, D.J.P., Burns, S.P., Monson, R.K., 2010. Longer growing seasons lead to less carbon sequestration by a subalpine forest. Glob. Chang. Biol. 16, 771–783. https://doi.org/10.1111/j.1365-2486.2009.01967.x.

Hubbard, R.M., Rhoades, C.C., Elder, K., Negron, J., 2013. Changes in transpiration and foliage growth in lodgepole pine trees following mountain pine beetle attack and mechanical girdling. For. Ecol. Manag. 289, 312–317. https://doi.org/10.1016/j.foreco.2012.09.028.

Hungerford, R.D., Nemani, R.R., Running, S.W., Coughlan, J.C., 1989. MTCLIM: A Mountain Microclimate Simulation Model (No. INT-RP-414). U.S. Department of Agriculture, Forest Service, Intermountain Forest and Range Experiment Station, Ogden, UT https://doi.org/10.2737/INT-RP-414.

Immerzeel, W.W., Lutz, A.F., Andrade, M., Bahl, A., Biemans, H., Bolch, T., Hyde, S., Brumby, S., Davies, B.J., Elmore, A.C., Emmer, A., Feng, M., Fernández, A., Haritashya, U., Kargel, J.S., Koppes, M., Kraaijenbrink, P.D.A., Kulkarni, A.V., Mayewski, P.A., Nepal, S., Pacheco, P., Painter, T.H., Pellicciotti, F., Rajaram, H., Rupper, S., Sinisalo, A., Shrestha, A.B., Viviroli, D., Wada, Y., Xiao, C., Yao, T., Baillie, J.E.M., 2020. Importance and vulnerability of the world's water towers. Nature 577, 364–369. https://doi.org/10.1038/s41586-019-1822-y.

Knowles, J.F., Burns, S.P., Blanken, P.D., Monson, R.K., 2015. Fluxes of energy, water, and carbon dioxide from mountain ecosystems at Niwot Ridge, Colorado. Plant Ecol.Divers. 8, 663–676. https://doi.org/10.1080/17550874.2014.904950.

Knowles, J.F., Lestak, L.R., Molotch, N.P., 2017. On the use of a snow aridity index to predict remotely sensed forest productivity in the presence of bark beetle disturbance. Water Resour. Res. 53, 4891–4906. https://doi.org/10.1002/2016WR019887.

Knowles, J.F., Molotch, N.P., Trujillo, E., Litvak, M.E., 2018. Snowmelt-driven trade-offs between early and late season productivity negatively impact forest carbon uptake during drought. Geophys. Res. Lett. 45, 3087–3096. https://doi.org/10.1002/2017GL076504.

Knowles, J.F., Scott, R.L., Biederman, J.A., Blanken, P.D., Burns, S.P., Dore, S., Kolb, T.E., Litvak, M.E., Barron-Gafford, G.A., 2020. Montane forest productivity across a semiarid climatic gradient. Glob. Chang.Biol. 26, 6945–6958. https://doi.org/10.1111/gcb.15335.

Koehn, C.R., Petrie, M.D., Bradford, J.B., Litvak, M.E., Strachan, S., 2021. Seasonal precipitation and soil moisture relationships across forests and woodlands in the southwestern United States. J Geophys. Res. Biogeosci. 126. https://doi.org/10.1029/2020JG005986.

Kool, D., Agam, N., Lazarovitch, N., Heitman, J.L., Sauer, T.J., Ben-Gal, A., 2014. A review of approaches for evapotranspiration partitioning. Agric. For. Meteorol. 184, 56–70. https://doi.org/10.1016/j.agrformet.2013.09.003.

Liang, L., Hawbaker, T.J., Zhu, Z., Li, X., Gong, P., 2016. Forest disturbance interactions and successional pathways in the Southern Rocky Mountains. For. Ecol. Manag. 375, 35–45. https://doi.org/10.1016/j.foreco.2016.05.010.

Liang, X., Lettenmaier, D.P., Wood, E.F., Burges, S.J., 1994. A simple hydrologically based model of land surface water and energy fluxes for general circulation models. J. Geophys. Res. 99, 14415. https://doi.org/10.1029/94JD00483.

Livneh, B., Bohn, T.J., Pierce, D.W., Munoz-Arriola, F., Nijssen, B., Vose, R., Cayan, D.R., Brekke, L., 2015a. A spatially comprehensive, hydrometeorological data set for Mexico, the U.S., and Southern Canada 1950–2013. Sci. Data 2, 150042. https://doi.org/10.1038/sdata.2015.42.

Livneh, B., Deems, J.S., Buma, B., Barsugli, J.J., Schneider, D., Molotch, N.P., Wolter, K., Wessman, C.A., 2015b. Catchment response to bark beetle outbreak and dust-on-snow in the Colorado Rocky Mountains. J. Hydrol. 523, 196–210. https://doi.org/10.1016/j.jhydrol.2015.01.039.

Maness, H., Kushner, P.J., Fung, I., 2012. Summertime climate response to mountain pine beetle disturbance in British Columbia. Nat. Geosci. 6, 65–70. https://doi.org/10.1038/ngeo1642.

Manning, A.L., Harpold, A., Csank, A., 2022. Spruce beetle outbreak increases streamflow from snow-dominated basins in Southwest Colorado, USA. Water Resour. Res. 58. https://doi.org/10.1029/2021WR029964.

Maxwell, R.M., Condon, L.E., 2016. Connections between groundwater flow and transpiration partitioning. Science 353, 377–380. https://doi.org/10.1126/science.aaf7891.

McDowell, N.G., Beerling, D.J., Breshears, D.D., Fisher, R.A., Raffa, K.F., Stitt, M., 2011. The interdependence of mechanisms underlying climate-driven vegetation mortality. Trends Ecol. Evol. 26, 523–532. https://doi.org/10.1016/j.tree.2011.06.003.

Mikkelson, K.M., Bearup, L.A., Maxwell, R.M., Stednick, J.D., McCray, J.E., Sharp, J.O., 2013. Bark beetle infestation impacts on nutrient cycling, water quality and interdependent hydrological effects. Biogeochemistry 115, 1–21. https://doi.org/10.1007/s10533-013-9875-8.

Mizukami, N., Clark, M.P., Newman, A.J., Wood, A.W., Gutmann, E.D., Nijssen, B., Rakovec, O., Samaniego, L., 2017. Towards seamless large-domain parameter estimation for hydrologic models. Water Resour. Res. 53, 8020–8040. https://doi.org/10.1002/2017WR020401.

Molotch, N.P., Blanken, P.D., Williams, M.W., Turnipseed, A.A., Monson, R.K., Margulis, S.A., 2007. Estimating sublimation of intercepted and sub-canopy snow using eddy covariance systems. Hydrol. Process. 21, 1567–1575. https://doi.org/10.1002/hyp.6719.

Monteith, J.L., 1973. Principles of Environmental Physics. Edward Arnold, London, U.K.

Moore, D.J., Trahan, N.A., Wilkes, P., Quaife, T., Stephens, B.B., Elder, K., Desai, A.R., Negron, J., Monson, R.K., 2013. Persistent reduced ecosystem respiration after insect disturbance in high elevation forests. Ecol. Lett. 16, 731–737.

Mu, Q., Zhao, M., Running, S.W., 2011. Improvements to a MODIS global terrestrial evapotranspiration algorithm. Remote Sens. Environ. 115, 1781–1800. https://doi.org/10.1016/j.rse.2011.02.019.

Nijssen, B., Lettenmaier, D.P., Liang, X., Wetzel, S.W., Wood, E.F., 1997. Streamflow simulation for continental-scale river basins. Water Resour. Res. 33, 711–724. https://doi.org/10.1029/96WR03517.

Nijssen, B., Schnur, R., Lettenmaier, D.P., 2001. Global retrospective estimation of soil moisture using the variable infiltration capacity land surface model, 1980–93. J. Clim. 14, 1790–1808. https://doi.org/10.1175/1520-0442(2001)014<1790:GREOSM>2.0.CO;2.

Norton, U., Ewers, B.E., Borkhuu, B., Brown, N.R., Pendall, E., 2015. Soil nitrogen five years after bark beetle infestation in lodgepole pine forests. Soil Sci. Soc. Am. J. 79, 282–293. https://doi.org/10.2136/sssaj2014.05.0223.

Paine, R.T., Tegner, M.J., Johnson, E.A., 1998. Compounded perturbations yield ecological surprises. Ecosystems 1, 535–545. https://doi.org/10.1007/s100219900049.

Potts, D.F., 1984. Hydrologic impacts of a large-scale mountain pine beetle (Dendroctonus ponderosae Hopkins) epidemic. J. Am. Water Resour. Assoc. 20, 373–377. https://doi.org/10.1111/j.1752-1688.1984.tb04719.x.

PRISM Climate Group, Oregon State University, 2021. https://prism.oregonstate.edu data created 17 Oct 2019, accessed 22 June 2021.

Pugh, E., Gordon, E., 2012. A conceptual model of water yield effects from beetle-induced tree death in snow-dominated lodgepole pine forests. Hydrol. Process. 27 (14), 2048–2060. https://doi.org/10.1002/hyp.9312.

Raffa, K.F., Aukema, B.H., Bentz, B.J., Carroll, A.L., Hicke, J.A., Kolb, T.E., 2015. Responses of tree-killing bark beetles to a changing climate. In: Björkman, C., Niemelä, P. (Eds.), Climate Change and Insect Pests. CABI, Wallingford, pp. 173–201 https://doi.org/10.1079/9781780643786.0173.

Reed, D.E., Ewers, B.E., Pendall, E., 2014. Impact of mountain pine beetle induced mortality on forest carbon and water fluxes. Environ. Res. Lett. 9, 105004. https://doi.org/10.1088/1748-9326/9/10/105004.

Reichstein, M., Falge, E., Baldocchi, D., Papale, D., Aubinet, M., Berbigier, P., Bernhofer, C., Buchmann, N., Gilmanov, T.G., Granier, A., Grünwald, T., Havránková, K., Ilvesniemi, H., Janous, D., Knohl, A., Laurila, T., Lohila, A., Loustau, D., Matteucci, G., Meyers, T., Miglietta, F., Ourcival, J.M., Pumpanen, J., Rambal, S., Rotenberg, E., Sanz, M., Tenhunen, J., Seufert, G., Vaccari, F., Vesala, T., Yakir, D., Valentini, R., 2005. On the separation of net ecosystem exchange into assimilation and ecosystem respiration: review and improved algorithm. Glob. Chang. Biol. 11, 1424–1439. https://doi.org/10.1111/j.1365-2486.2005.001002.x.

Ren, J., Adam, J.C., Hicke, J.A., Hanan, E.J., Tague, C.L., Liu, M., Kolden, C.A., Abatzoglou, J.T., 2021. How does water yield respond to mountain pine beetle infestation in a semiarid forest? Hydrol. Earth Syst. Sci. 25, 4681–4699. https://doi.org/10.5194/hess-25-4681-2021.

Rhoades, C.C., McCutchan Jr., J.H., Cooper Jr., L.A., Clow Jr., D., Detmer Jr., T.M., Briggs Jr., J.S., Stednick Jr., J.D., Veblen Jr., T.T., Ertz Jr., R.M., Likens Jr., G.E., Lewis Jr., W.M., 2013. Biogeochemistry of beetle-killed forests: explaining a weak nitrate response. Proc. Natl. Acad. Sci. 110, 1756–1760. https://doi.org/10.1073/pnas.1221029110.

Roberts, J., 1983. Forest transpiration: a conservative hydrological process? J. Hydrol. 66, 133–141. https://doi.org/10.1016/0022-1694(83)90181-6.

Rodman, K., Andrus, R.A., Carlson, A.R., Carter, T.A., Chapman, T.B., Coop, J.D., Fornwalt, P.J., Gill, N.S., Harvey, B.J., Hoffman, A.E., Kelsey, K.C., Kulakowski, D., Laughlin, D.C., Morris, J.E., Negrón, J.F., Nigro, K.M., Pappas, G.S., Redmond, M.D., Rhoades, C.C., Rocca, M.E., Schapira, Z.H., Sibold, J.S., Stevens-Rumann, C.S., Veblen, T.T., Wang, J., Zhang, X., Hart, S., 2022. Rocky Mountain forests are poised to recover following bark beetle outbreaks but with altered composition. J. Ecol. https://doi.org/10.1111/1365-2745.13999.

Running, S., Mu, Q., Zhao, M., Moreno, A., 2019. MOD16A2GF MODIS/Terra Net Evapotranspiration Gap-Filled 8-Day L4 Global 500 m SIN Grid V006. distributed by NASA EOSDIS Land Processes DAAC https://doi.org/10.5067/MODIS/MOD16A2GF.006 Accessed 2020-06-03.

Scott, R.L., Knowles, J.F., Nelson, J.A., Gentine, P., Li, X., Barron-Gafford, G., Bryant, R., Biederman, J.A., 2021. Water availability impacts on evapotranspiration partitioning. Agric. For. Meteorol. 297, 108251. https://doi.org/10.1016/j.agrformet.2020.108251.

Sexstone, G.A., Clow, D.W., Fassnacht, S.R., Liston, G.E., Hiemstra, C.A., Knowles, J.F., Penn, C.A., 2018. Snow sublimation in mountain environments and its sensitivity to forest disturbance and climate warming. Water Resour. Res. 54, 1191–1211. https://doi.org/10.1002/2017WR021172.

Shuttleworth, J.W., 1993. Evaporation. In: Maidment, D.R. (Ed.), Handbook of Hydrology. McGraw-Hill, New York, pp. 4.1–4.53.

Slinski, K.M., Hogue, T.S., Porter, A.T., McCray, J.E., 2016. Recent bark beetle outbreaks have little impact on streamflow in the Western United States. Environ. Res. Lett. 11, 074010. https://doi.org/10.1088/1748-9326/11/7/074010.

Speckman, H.N., Frank, J.M., Bradford, J.B., Miles, B.L., Massman, W.J., Parton, W.J., Ryan, M.G., 2014. Forest ecosystem respiration estimated from eddy covariance and chamber measurements under high turbulence and substantial tree mortality from bark beetles. Glob. Chang. Biol. 21, 708–721. https://doi.org/10.1111/gcb.12731.

Stednick, J.D., 1996. Monitoring the effects of timber harvest on annual water yield. J. Hydrol. 176, 79–95. https://doi.org/10.1016/0022-1694(95)02780-7.

Sterling, S.M., Ducharne, A., Polcher, J., 2012. The impact of global land-cover change on the terrestrial water cycle. Nat. Clim. Chang. 3, 385–390. https://doi.org/10.1038/nclimate1690.

Tai, X., Mackay, D.S., Ewers, B.E., Parsekian, A.D., Beverly, D., Speckman, H., Brooks, P.D., Anderegg, W.R.L., 2019. Plant hydraulic stress explained tree mortality and tree size explained beetle attack in a mixed conifer forest. J. Geophys. Res. Biogeosci. 124, 3555–3568. https://doi.org/10.1029/2019JG005272.

Thayer, D., Parsekian, A.D., Hyde, K., Speckman, H., Beverly, D., Ewers, B., Covalt, M., Fantello, N., Kelleners, T., Ohara, N., Rogers, T., Holbrook, W.S., 2018. Geophysical measurements to determine the hydrologic partitioning of snowmelt on a snow-dominated subalpine hillslope. Water Resour. Res. 54, 3788–3808. https://doi.org/10.1029/2017WR021324.

Tian, Y., Dickinson, R.E., Zhou, L., Zeng, X., Dai, Y., Myneni, R.B., Knyazikhin, Y., Zhang, X., Friedl, M.A., Yu, H., Wu, W., Shaikh, M., 2004. Comparison of seasonal and spatial variations of leaf area index and fraction of absorbed photosynthetically active radiation from Moderate Resolution Imaging Spectroradiometer (MODIS) and common land model. J. Geophys. Res. 109, D01103. https://doi.org/10.1029/2003JD003777.

Turnipseed, A.A., Blanken, P.D., Anderson, D.E., Monson, R.K., 2002. Energy budget above a high-elevation subalpine forest in complex topography. Agric. For. Meteorol. 110, 177–201. https://doi.org/10.1016/S0168-1923(01)00290-8.

Ukkola, A.M., Prentice, I.C., Keenan, T.F., van Dijk, A.I.J.M., Viney, N.R., Myneni, R.B., Bi, J., 2015. Reduced streamflow in water-stressed climates consistent with CO2 effects on vegetation. Nat. Clim. Chang. 6, 75–78. https://doi.org/10.1038/nclimate2831.

United States (US) Environmental Protection Agency (EPA), 2010. Level III Ecoregions of the Continental United States. U.S. EPA National Health and Environmental Effects Research Laboratory, Map M-1, Various Scales, Corvallis, OR.

Vanderhoof, M.K., Williams, C.A., 2015. Persistence of MODIS evapotranspiration impacts from mountain pine beetle outbreaks in lodgepole pine forests, south-central Rocky

Mountains. Agric. For. Meteorol. 200, 78–91. https://doi.org/10.1016/j.agrformet.2014.09.015.

Viviroli, D., Archer, D.R., Buytaert, W., Fowler, H.J., Greenwood, G.B., Hamlet, A.F., Huang, Y., Koboltschnig, G., Litaor, M.I., López-Moreno, J.I., Lorentz, S., Schädler, B., Schreier, H., Schwaiger, K., Vuille, M., Woods, R., 2011. Climate change and mountain water resources: overview and recommendations for research, management and policy. Hydrol. Earth Syst. Sci. 15, 471–504. https://doi.org/10.5194/hess-15-471-2011.

Wei, Z., Yoshimura, K., Wang, L., Miralles, D.G., Jasechko, S., Lee, X., 2017. Revisiting the contribution of transpiration to global terrestrial evapotranspiration: revisiting global ET partitioning. Geophys. Res. Lett. 44, 2792–2801. https://doi.org/10.1002/2016GL072235.

Wieder, W.R., Knowles, J.F., Blanken, P.D., Swenson, S.C., Suding, K.N., 2017. Ecosystem function in complex mountain terrain: combining models and long-term observations to advance process-based understanding: alpine ecosystem function and insight. J. Geophys. Res. Biogeosci. 122, 825–845. https://doi.org/10.1002/2016JG003704.

Winchell, T.S., Barnard, D.M., Monson, R.K., Burns, S.P., Molotch, N.P., 2016. Earlier snowmelt reduces atmospheric carbon uptake in midlatitude subalpine forests. Geophys. Res. Lett. 43, 8160–8168. https://doi.org/10.1002/2016GL069769.

Wulder, M.A., Dymond, C.C., White, J.C., Leckie, D.G., Carroll, A.L., 2006. Surveying mountain pine beetle damage of forests: a review of remote sensing opportunities. For. Ecol. Manag. 221, 27–41. https://doi.org/10.1016/j.foreco.2005.09.021.

Wutzler, T., Lucas-Moffat, A., Migliavacca, M., Knauer, J., Sickel, K., Šigut, L., Menzer, O., Reichstein, M., 2018. Basic and extensible post-processing of eddy covariance flux data with REddyProc. Biogeosciences 15, 5015–5030. https://doi.org/10.5194/bg-15-5015-2018.

Zhou, S., Yu, B., Huang, Y., Wang, G., 2014. The effect of vapor pressure deficit on water use efficiency at the subdaily time scale. Geophys. Res. Lett. 41, 5005–5013. https://doi.org/10.1002/2014GL060741.

Zhou, S., Yu, B., Zhang, Y., Huang, Y., Wang, G., 2016. Partitioning evapotranspiration based on the concept of underlying water use efficiency. Water Resour. Res. 52, 1160–1175. https://doi.org/10.1002/2015WR017766.